Mixing of immiscible liquids

Mixing and Compounding – Theory and Practice

Vol. eds.: I. Manas–Zloczower and Z. Tadmor

Progress in Polymer Processing Series

Series ed.: L.A. Utracki

Section I.4:

MIXING OF IMMISCIBLE LIQUIDS

by

Han E.H. Meijer, Jos M.H. Janssen

July 1992

WFW report nr. 92.080

Eindhoven University of Technology

Centre for Polymers and Composites

P.O. Box 513, 5600 MB Eindhoven

The Netherlands

Summary

In this section the literature on the mixing of immiscible liquids is reviewed. It is shown that well–defined experiments, restricted by a number of simplifying assumptions and describing isolated elementary steps of the mixing process, are helpful and illustrative for the understanding of practical mixing problems.

The modelling of the basic processes starts with large dispersed drops and thus at Capillary numbers much larger than Ca_{crit} (i.e. the critical ratio between the (deforming) shear stress and the (conservative) interfacial stress, above which no stable equilibrium drop shape exists). In that case, the interfacial stress is overruled by the shear stress (passive interfaces) and the (simple) principles of distributive mixing emerge, where deformation rate and time are interchangeable. Stretching and folding in a periodic flow should be realized for efficient mixing and the occurence of regular islands is to be avoided. The mathematical tools are available to numerically model distributive mixing even in 3–D transient flows, although the necessary computing time could be a constraint.

As the local lengthscale decreases during the mixing process, the interfacial stress becomes of the same order as the shear stress ($Ca \simeq Ca_{crit}$) and the long slender bodies formed disintegrate into lines of small droplets (dispersive mixing). Interfaces are active and deformation rate and time are each important. Therefore, in transient flows the timescales of the competitive processes of deformation of the filaments, retraction, endpinching, and growth of interfacial disturbances, determine the size of the resulting dispersed fragments. Also for these problems numerical models have been derived.

For large local deformations viscoelasticity has a pronounced effect on the typical timescales of the distinct processes, due to the orientation of the macromolecules, and thus influences the final morphology of the system. More research is needed in this area. The same holds for coalescence, which causes a coarsening of the morphology. The final average dropsize can be considered a result of a dynamic equilibrium between breakup and coalescence. For high volumefractions of the dispersed phase or low values of the viscosity ratio between dispersed phase and matrix, phase inversion can occur. A promising analogy of these processes, which complicate the extrapolation from single step experiments with model liquids to application to practical polymer blending, could be found in recent results of the computer modelling of the rheology of foam.

Contents

Summary

Contents

4.1. Introduction

In polymer technology two main routes can be discerned in order to reach specific material properties that homopolymers often cannot accomplish (e.g., a high notched impact strength combined with a reasonable modulus and continuous use temperature necessary for engineering applications of polymers). One way is to blend or modify polymers in the reactor (in situ), like (block) copolymerization of for example Polyurethanes (PUR), Styrene–Butadiene–Styrene block copolymers (SBS), Reactor Modified Polypropylene (RMPP), High Impact Polystyrene (HIPS), and Acrylonitrile–Butadiene–Styrene (ABS). The other way is the (extrusion) melt blending of different existing (homo)polymers. The versatility of melt blending techniques offers some advantages over the more traditional reactor modification. In reactive extrusion, moreover, in situ blending is promoted by specific reactions at the interface.

Since most polymer combinations of interest are thermodynamically immiscible on a molecular scale, a specific microstructure of the separate phases results from the melt blending process; this morphology partly determines the final properties of the blend. In Figure 4.1, some examples of such morphologies are given for the model–system Polystyrene (PS) / High Density Polyethylene (HDPE).

At the end of the melt blending process the morphology, which is not necessarily in an equilibrium state, is frozen–in in the solid state. In a subsequent processing step, such as injection moulding or film blowing, the morphology achieved may be altered due to the typical processing conditions there. Since the resulting morphology depends on the processing technique and conditions, the volume fractions and viscosity ratio of the polymers, the meltelasticity and most important the time of mixing, it is of great concern to model the mixing process in a principally transient approach. However, since polymer

blending involves complex, non–isothermal, non–Newtonian, time dependent flows, direct research on industrial compounding equipment generally yields compound– and machine limited results which might be useful for the specific problem under investigation, but are not conclusive in a more general sense.

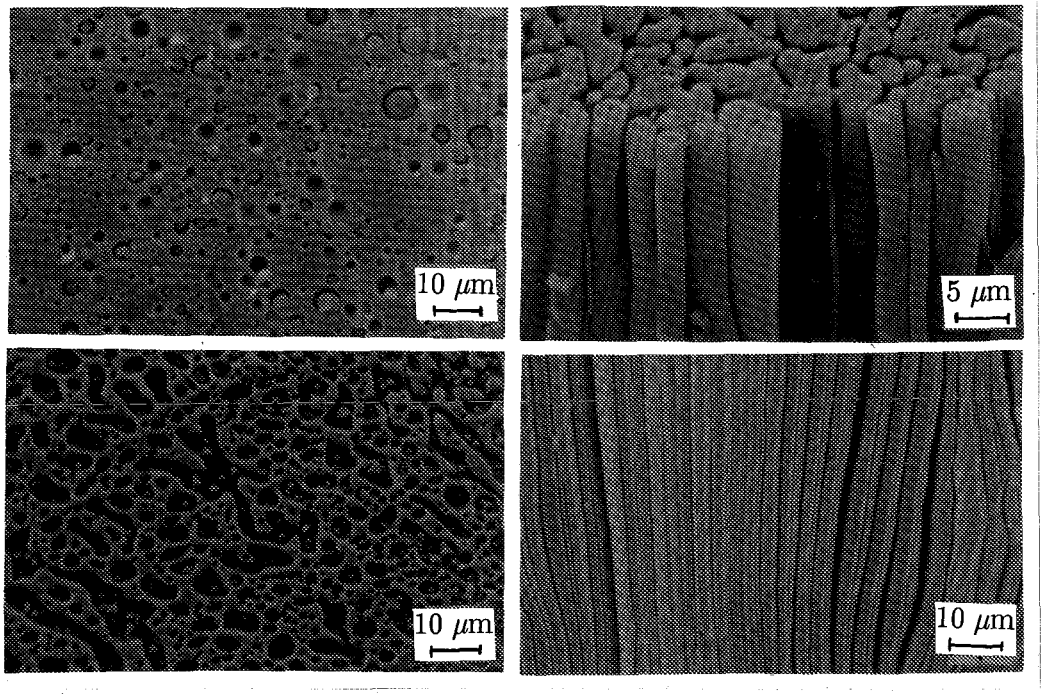

Figure 4.1 *Morphologies of some blends of PS and HDPE: spheres or fibers in a matrix, a cocontinuous, and a lamellar structure (Meijer et al. 1988). Reprinted with permission of Hüthig und Wepf Verlag.*

As a consequence, most of the fundamental research on the mixing of immiscible liquids has been focussed on idealized systems: using single drops of Newtonian model liquids in well–defined flow fields at roomtemperature. The results of this research are generally given in dimensionless representation and are scaled to practical processes in the areas of, for example, polymer blending and foodtechnology.

4.2. Mixing Mechanisms

In the mixing of immiscible liquids, e.g. in polymer blending, the minor component is generally present as the dispersed phase (drops or filaments) in a continuous phase of the major component. An elementary step in the mixing process is the deformation of dispersed drops in the flow field, yielding an increase in the interfacial area between the two components accompanied by a decrease in local dimensions perpendicular to the flow direction: the striation thickness. The interfacial area and the striation thickness both can be used as a measure for the quality of mixing. Deformation of drops is promoted by the shear stress τ exerted on the drops by the flow field and counteracted by the interfacial stress σ/R (with σ the interfacial tension and R the local radius) minimizing the surface to volume ratio, thus tending to a spherical shape. The ratio between these two stresses is called the Capillary number Ca:

$$\mathrm{Ca} = \frac{\tau\ \mathrm{R}}{\sigma} \tag{4.1}$$

Sometimes in the literature, the ratio between shear stress and interfacial stress is referred to as the Weber number. According to Catchpole and Fulfort (1988), four different Weber numbers, two Capillarity numbers, and one Capillary number may be defined, depending on the process under consideration. Weber number 1 relates inertia to the interfacial stress:

$$We_1 = \frac{\rho\ U^2 L}{\sigma} \tag{4.2}$$

with ρ the density, U the characteristic velocity, and L the characteristic lengthscale (for example the local radius R of a drop). Since the Reynolds number represents the ratio between inertia and viscous stress:

$$Re = \frac{\rho\ U\ L}{\eta} \qquad (4.3)$$

the Capillary number (Equation 4.1) equals:

$$Ca = We_1 / Re \qquad (4.4)$$

where the (viscous) shear stress exerted on the drop is expressed as $\tau = \eta\ U/\ R$. Generally, in the mixing of immiscible liquids, especially molten polymers, the Reynolds number is small and the interfacial stress (σ/R) should be compared to the shear stress (τ), with neglect of inertia. Therefore the Capillary number is the relevant dimensionless number. In the case of liquid drops or threads in a gas medium, Reynolds may be larger so that the interfacial stress (σ/R) should be compared to inertia ($\rho\ U^2$) and Weber number 1 is the governing number.

If the Capillary number exceeds a critical value, Ca_{crit}, the viscous shear stress overrules the interfacial stress, no stable equilibrium drop shape exists, the drop is extended and finally will breakup into smaller droplets. If $Ca < Ca_{crit}$, the interfacial stress competes with the shear stress and the drop will only slightly deform in the flow field, yielding a stable drop shape. Taylor (1932, 1934) was the first to, theoretically and experimentally, investigate the critical conditions for breakup of dispersed drops.

Taylor originally attempted to predict the viscosity of an emulsion, a liquid containing deformable drops of another (immiscible) liquid, via an extension of Einstein's (1906, 1911) relation for the viscosity of a suspension, a liquid containing rigid spheres:

$$\eta = \eta_0\ (1 + 2.5\,\phi) \qquad (4.5)$$

with ϕ the volumefraction of rigid spheres and η_0 the viscosity of the surrounding liquid. As Einstein's goal was not so much to initiate the dispersion rheology (his aim was to obtain, from viscosity measurements in a dilute solution, quantitative information on the radius of gyration of molecules), Taylor did not intend to give a start to the modelling of dispersive mixing. Via a calculation of the flow inside and around a dispersed liquid drop, Taylor (1932) derived the expression:

$$\eta = \eta_0 \left(1 + 2.5\,\phi \left[\frac{p + 2/5}{p + 1}\right]\right) \qquad (4.6)$$

with

$$p = \eta_d / \eta_c \qquad (4.7)$$

the viscosity ratio between the dispersed and the continuous (matrix) phase, which for $p \to \infty$ renders Einstein's original result. In order to verify his assumption that the drop would stay almost spherical, Taylor had to investigate under which circumstances a drop would severely deform and breakup. The results of this research, the genuine start of the modelling of dispersive mixing, were published in 1934.

Taylor found that, in simple shear flow, a dispersed drop with viscosity ratio p = 1 becomes unstable and breaks up if Ca > 0.5, thus Ca_{crit} is of the order unity. Apparently, breakup occurs when both competitive stresses (τ and σ/R) are of the same order of magnitude. Ca_{crit} depends on the type of flow, simple shear versus elongational flow, and on the viscosity ratio p, see below in Figures 4.26 and 4.34. Also the rate of drop deformation and the time to breakup strongly depend on p. All microrheological processes generally occur faster for low viscous drops in a highly viscous continuous phase (p < 1) than in the opposite case (p > 1).

A useful subdivision of the mixing process can be based on the value of the (local) Capillary number, which continuously decreases during the process, due to the decrease of the typical lengthscale (in polymer blending roughly from 1 mm to 1 μm):

(i) Distributive mixing when Ca >> Ca_{crit} (large dispersed domains, passive interfaces); drops are extended affinely with the matrix but do not develop capillary waves leading to breakup, since the interfacial stress is overruled by the shear stress.

(ii) Dispersive mixing when Ca $\simeq$ Ca_{crit} (locally small radii of curvature, active interfaces); σ/R competes with τ and causes disturbances at the interface to grow, leading to breakup into smaller droplets and thus to a finer dispersion.

Although in reality distributive and dispersive mixing do not occur separately in a mixing device (see, e.g., Figure 4.38), this distinction is useful for a better understanding of the mixing process.

Apart from a tendency towards finer morphologies resulting from distributive and dispersive mixing, a coarsening of the morphology may occur during mixing due to coalescence of the dispersed droplets. As is indicated in Paragraph 4.5, coalescence preferentially takes place at almost quiescent regions of the flow, in contrast to the two mixing mechanisms described above. In the next paragraphs distributive mixing, dispersive mixing, and coalescence are discussed subsequently.

4.3. Distributive Mixing ($Ca >> Ca_{crit}$)

4.3.1 Affine Deformation

Recently, some attention has been given to lamellar starting morphologies for the mixing process, see e.g. Ghosh et al. (1991). These stratified structures originate from the melting process of polymers in an extruder, characterized by drag removal. Sheets of the dispersed phase become unstable and break up into threads, which then may break up into drops. Here however, a drop in matrix structure, with the dropsize of the same order of magnitude as the granular polymeric feedstock (~ 1 mm), is considered as a typical starting morphology. This dropsize might be considered as an upper bound in terms of the characteristic lengthscale. For immiscible polymer melts, an order of magnitude estimate of the local Capillary number yields:

$$\left.\begin{aligned} \tau &= \eta_c \dot{\gamma} = 10^2 \cdot 10^2 = 10^4 \text{ Pa} \\ \sigma/R &= 10^{-2} / 10^{-3} = 10 \text{ Pa} \end{aligned}\right\} \quad Ca = \frac{\eta_c \dot{\gamma} R}{\sigma} = 10^3 \qquad (4.8)$$

with

τ = shear stress [Pa]

η_c = viscosity continuous phase [Pa·s]

$\dot{\gamma}$ = shear rate [s^{-1}], (defined in Paragraph 4.4.5)

σ = interfacial tension [N/m]

R = drop radius [m]

Note that in Equation 4.8 the Newtonian constitutive equation is substituted; the knowledge of the mixing process is largely limited to the mixing of Newtonian liquids. From Equation 4.8 it follows that $Ca >> Ca_{crit}$ since $Ca_{crit} \approx 1$. Consequently, the

conservative interfacial stress (σ/R) is overruled by the deforming shear stress and the (millimeter sized) drops deform affinely with the matrix, i.e. distributive mixing with passive interfaces. Note that for miscible liquids (no interfacial tension) distributive mixing is the only process of interest (apart, of course, from diffusion).

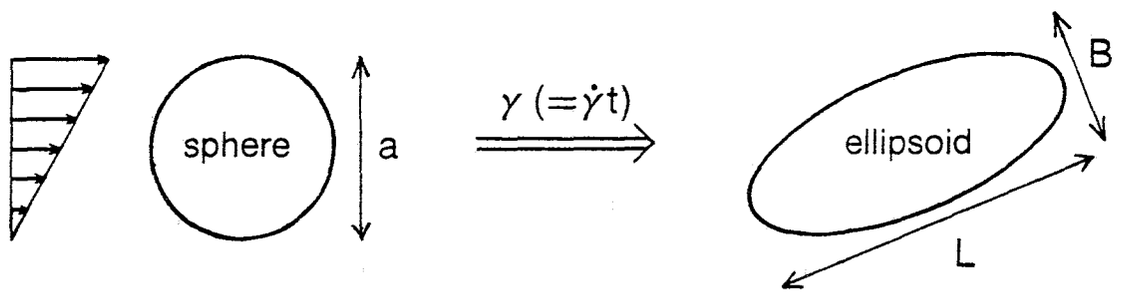

Figure 4.2 *Affine deformation of a liquid drop in simple shear flow.*

Figure 4.2 illustrates the affine deformation in simple shear flow of a sphere with diameter 'a' (=2R) into an ellipsoid with length L and width B. The extent of drop deformation is defined as:

$$D = \frac{L - B}{L + B} \tag{4.9}$$

and changes from 0 (sphere) to 1 (infinitely extended thread). The drop deformation can be calculated from the eigenvalue problem of the right Cauchy–Green tensor **C** (= $\mathbf{F}^c \cdot \mathbf{F}$, with **F** the deformation tensor). In simple shear flow this yields:

$$L/a = \left[1 + \frac{\gamma^2}{2} + \frac{\gamma}{2}\sqrt{4+\gamma^2}\right]^{1/2} \tag{4.10}$$

$$B/a = \left[1 + \frac{\gamma^2}{2} + \frac{\gamma}{2}\sqrt{4+\gamma^2}\right]^{-1/4} \tag{4.11}$$

$$D = \frac{\left[1 + \frac{\gamma^2}{2} + \frac{\gamma}{2}\sqrt{4+\gamma^2}\right]^{3/4} - 1}{\left[1 + \frac{\gamma^2}{2} + \frac{\gamma}{2}\sqrt{4+\gamma^2}\right]^{3/4} + 1} \tag{4.12}$$

which can be simplified for total shear values $\gamma \geq 5$:

$$L/a \approx \gamma \tag{4.13}$$

$$B/a \approx \gamma^{-1/2} \tag{4.14}$$

$$D \approx \frac{\gamma^{3/2} - 1}{\gamma^{3/2} + 1} \tag{4.15}$$

The affine deformation of a drop is a function of the total shear γ ($= \dot{\gamma}t$) only. The shear rate $\dot{\gamma}$ and the time t are completely interchangeable, thus a slow deformation during a long time will give exactly the same result as a fast deformation during a short time, provided that the total shear remains constant.

Note that a lower limit for the shear rate $\dot{\gamma}$ is present because always $Ca >> Ca_{crit}$ must be fulfilled. Moreover, in simple shear, affine deformation can only be realized if $p < 4$. This additional limitation follows from the fact that for higher values of the viscosity ratio, the critical Capillary number for drop breakup goes to infinity, see Figure 4.26.

In simple shear flow the relative length L/a almost linearly increases with the total shear γ. As will be shown in the next paragraph, this is not a very efficient way of mixing.

In elongational flow, the length of an affinely deforming drop increases exponentially:

$$L/a = e^{\epsilon} \tag{4.16}$$

$$B/a = e^{-\epsilon/2} \tag{4.17}$$

$$D = \frac{e^{3\epsilon/2} - 1}{e^{3\epsilon/2} + 1} \tag{4.18}$$

Once more, only the total strain is important: $\epsilon = \dot{\epsilon}t$, the product of the elongation rate $\dot{\epsilon}$ and time. As demonstrated in Figure 4.3, in elongational flow L/a and D increase much faster than in simple shear.

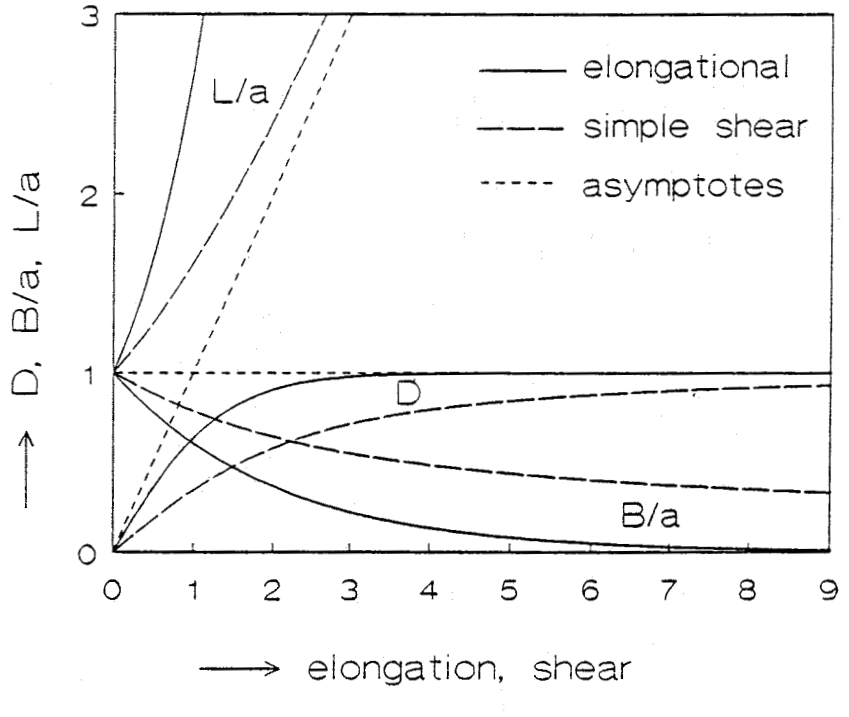

Figure 4.3 *Progress of affine deformation in simple shear and elongational flow.*

In elongational flow the elongated drop remains oriented in the direction of the principal axis of strain, while in simple shear the drop rotates towards the direction of the streamlines. This is the principal difference between so–called strong (mainly irrotational) and weak (mainly rotational) flows. The presence of rotation in simple shear flow is also responsible for the more complicated expressions for affine drop deformation (compare Equations 4.10–4.12 to 4.16–4.18). The practical problem in realising efficient irrotational flows, like unidirectional extension, is that it is quite impossible to sustain these flows long enough to realize a sufficient total strain (convergencies are either finite or yield no throughput).

4.3.2 Efficient Mixing: Folding and Reorienting

The main difference between (irrotational) elongation and (partially rotational) simple shear can also be seen from the efficiency parameter e_f, defined as the scalar product of the principal direction of strain and the transient drop orientation. Figure 4.4 illustrates the change of the efficiency e_f with increasing deformation in different flows.

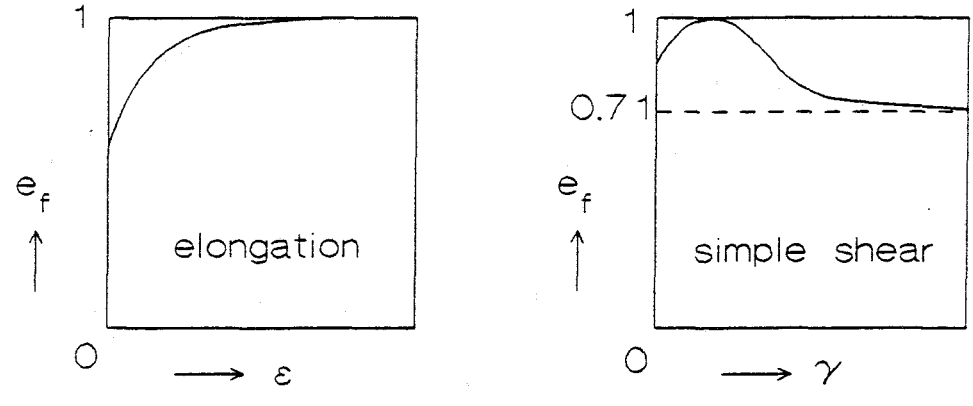

Figure 4.4 *Efficiency e_f (scalar product of the principal direction of strain and the drop orientation) for an arbitrary initial orientation.*

In elongation the efficiency e_f approaches 1, irrespective of the initial orientation (the drop tends to orient along the principal axis of strain), while in simple shear e_f shortly reaches a value of 1, when the orientation of the drop is at 45^0 relative to the direction of the velocity gradient (45^0 is the principal direction of strain in simple shear), but ultimately approaches $1/\sqrt{2}$ caused by the rotation of the extended drop to the direction of the flow. By repeatedly reorienting extended drops in simple shear, with their main axis perpendicular to the streamlines, this maximum ($e_f = 1$) can be obtained more than once, yielding a more efficient mixing process. However, only a combination of folding and reorienting changes the efficiency of the distributive mixing from a linear dependence on the total shear into an exponential dependence. The principle of this "stretching and folding" mechanism is depicted schematically in Figure 4.5. To maintain the interfacial area gained, the surface of the stretched material should, of course, be surrounded by matrix material.

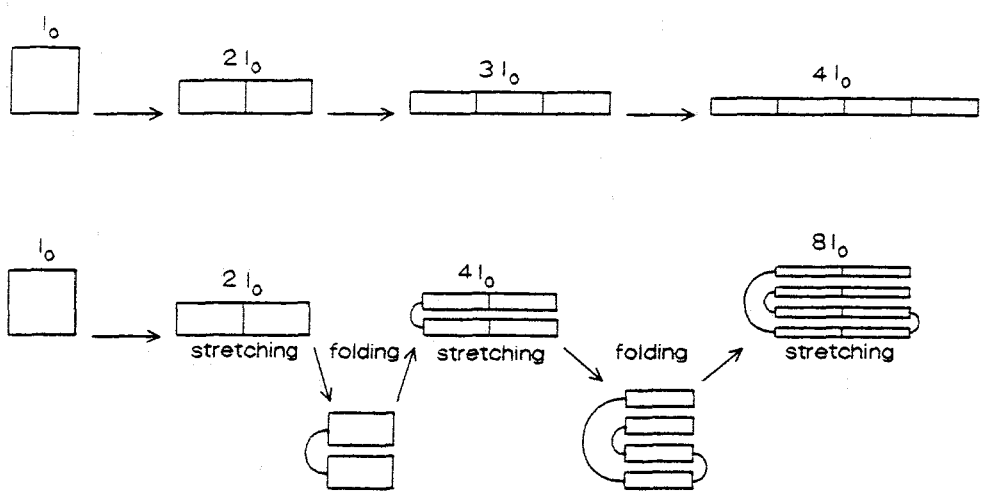

Figure 4.5 *Stretching and folding during distributive mixing; the material is folded after every extension equal to the initial length l_0 (baker's transformation).*

This transformation, resulting in the exponential way of mixing, is familiar to housewives. It is called the baker's transformation, named after the way dough is mixed by repeatedly rolling (which is a stretching operation) and folding.

In the past, when the maximum attainable temperature in ovens (ca. 1100 ^0C) was below the melting point of iron (ca. 1500 ^0C), iron could only be separated from the ore because melting temperature depression occurred, caused by the diffusion of carbon from the cokes in the furniture. Cast iron resulted with inferior mechanical properties. Upgrading to steel proved to be possible via oxydative removal of the extra carbon in the iron by forging. During forging, the iron is heated, hammered (which is stretching), folded, heated again, and so on. In this way, the striation thickness, which is the typical distance for diffusion of oxygen and carbondioxide, is efficiently decreased, while the surface area is increased. Good steel required a 5000 times repetition of this baker's transformation, which apparently has been known for a long time, see Gordon (1968, 1978).

Ng and Erwin (1981) performed experiments, using polymers, to illustrate the efficiency of the baker's transformation in a Couette flow. By alternating black and white coloured strokes of the same polymer in the gap between two concentric rotors, see Figure 4.6, and (after melting) rotating one of the cylinders over a total angle γ_{tot}, mixing is visualized. Quantitatively, the mixing efficiency can be measured and calculated with the striation thickness, the total number of layers or the total interfacial area A:

$$\frac{A}{A_0} \sim \gamma_{tot} \qquad (4.19)$$

By dividing the total shear γ_{tot} in n equal intervals and reorienting the flow, once a shear of γ_{tot}/n is reached, in a perfect manner (by cutting the ring into square pieces and

subsequently rotating every individual piece over 90^0), the interfacial area increases exponentially with shear:

$$\frac{A}{A_0} \sim \left[\frac{\gamma_{tot}}{n}\right]^n \qquad (4.20)$$

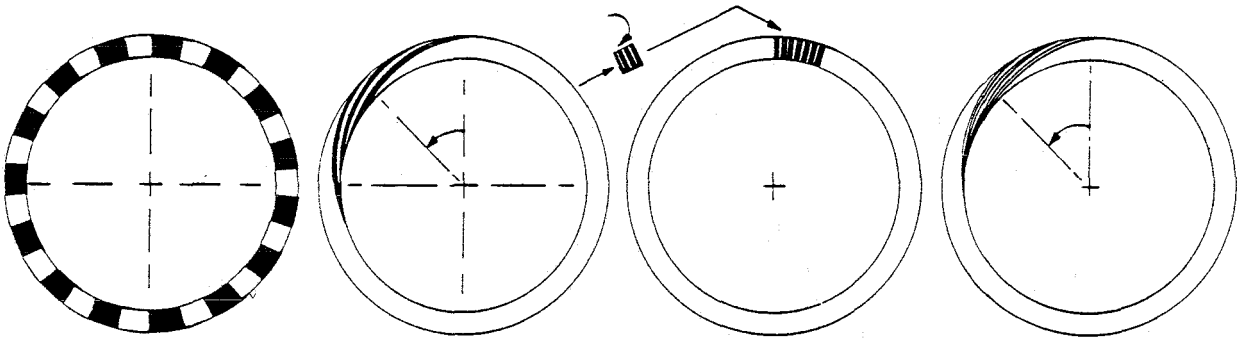

Figure 4.6 *Shear with reorientation of black and white segments (after Ng and Erwin 1981).*

Distributive mixing can be summarized as (i) affine deformation, with no influence of the interfacial tension (passive interfaces), (ii) stretching, with equivalency of shear rate and time, since only the total shear is important, and (iii) folding and reorienting, which yields the exponential mixing coefficient n.

4.3.3 Static Mixers

A perfect illustration of the application of the efficient baker's transformation in practical mixing is realized in almost all well–designed static mixers. The working principle of a static mixer is based on the stretching and folding mechanism illustrated in Figure 4.5. Three major steps can be distinguished (Figure 4.7): stretching, cutting and stacking. The last two steps are equivalent to the folding in Figure 4.5.

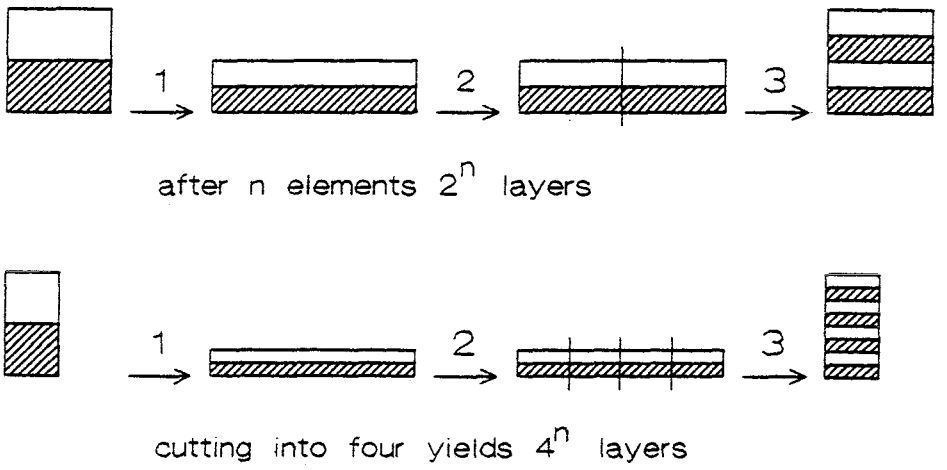

Figure 4.7 *Working principle of static mixers: 1) stretching, 2) cutting, 3) stacking.*

Multiflux

Primus inter pares of all static mixers is the Multiflux mixer, originally developed by Akzo, see Sluijters (1965) and Schilo and Ostertag (1972). By acceleration and deceleration between trapezoidal shaped blocks the material is stretched, cut, and stacked. As can be seen in Figure 4.8, this mixer almost ideally approaches the theoretical baker's transformation and yields 2^n layers, n being the number of elements.

In their book "Order out of Chaos" (1984), which tries to give an answer to the apparent contradiction between the (optimistic) evolution law and the (pessimistic) second law of thermodynamics via a "far from equilibrium" approach, Prigogine and Stengers use the principle of Figure 4.8 to illustrate the influence of the initial configuration on a general transient process. They consider the development of a mathematical line, which is something with a length but without any width, during a repetitive baker's transformation. Consequently, the initial configuration of the line determines what will happen in time: a vertical line yields a completely different result compared to a horizontal line, since the first will cover the total available area while the second will vanish. In an experiment obeying conservation of mass, however, the first transformation continuously transfers into the second and vice versa.

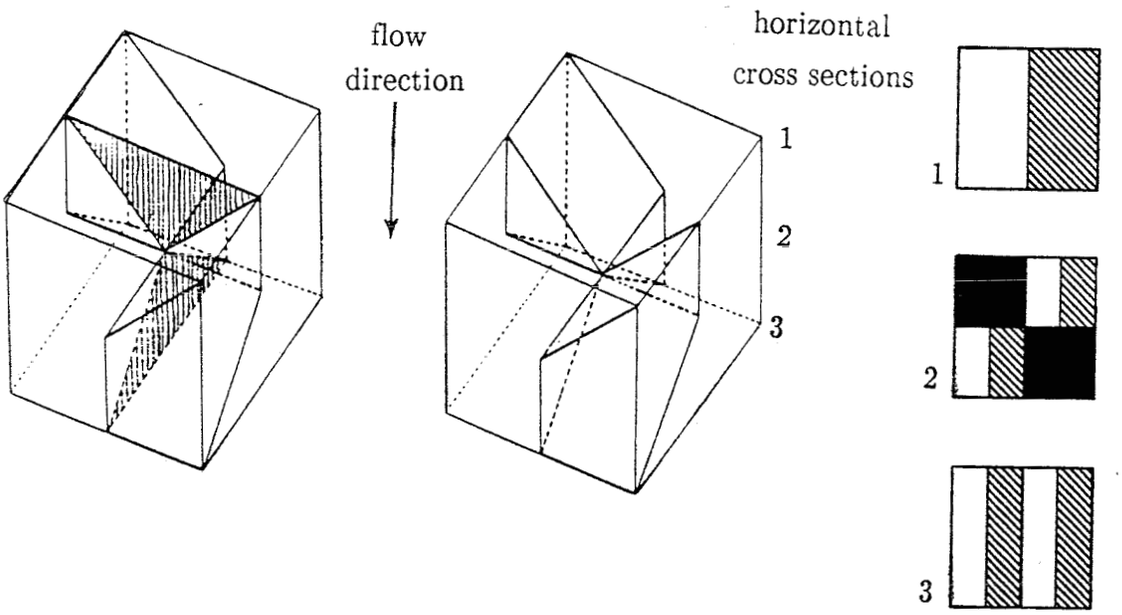

Figure 4.8 *The Multiflux static mixer (Akzo); schematically.*

Ross

The second static mixer, which closely approaches the ideal working principle of the baker's transformation, is the Ross ISG (interfacial surface generator), developed by DOW, see Figure 4.9.

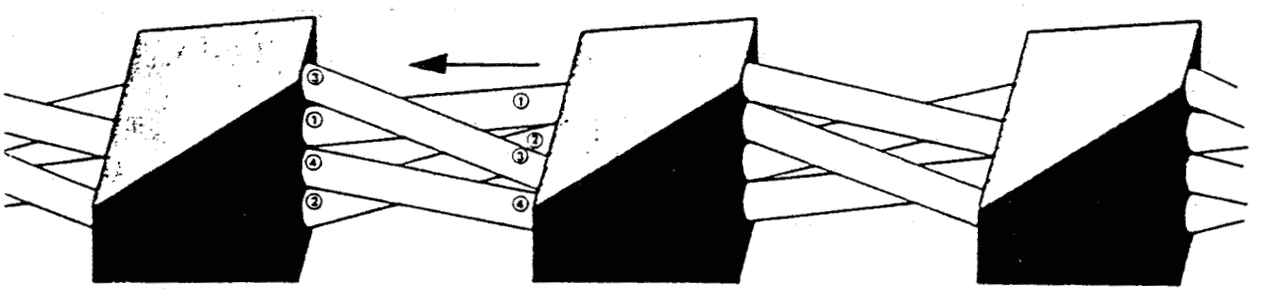

Figure 4.9 *The Ross (ISG) static mixer; outside view only.*

Stretching takes place inside the trapezoidal shaped blocks, cutting during the inflow in the four small tubes and, finally, stacking is realized by the twist of the tubes. Because there are four tubes, 4^n layers result after n elements.

Sulzer

One of the most complex static mixers is, without doubt, the Sulzer mixer. Seemingly, the interior part looks like randomly stacked wirenetting, although the distinct elements are consistently and alternatingly rotated over 90^0. Publications on this mixer, mostly originating from the manufacturer, repeatedly show the experimental result of the one split mixer, fed with a differently coloured polymer and longitudinally cut into two halves after quenching, which proves that the mixer works. The flow inside is, however, much less well defined compared to the two mixers already discussed. An outline of the working principle is given in Figure 4.10. Two crossed screens form the basis of one element. Fed by a black and a white liquid, half of the black material flows through the openings in the lower part of the screen while half of it runs along the screen towards the top half (stretching). For the white material, the opposite occurs. Subsequently, the black and white material have to flow around the last obstacles, where the white cuts the black (and vice versa) and stacking takes place. From the schematic representation of the flow in Figure 4.10, it is clear why the next element has to be rotated over 90^0. Because in the example the flow is split into four streams, 4^n layers result.

All static mixers discussed, make use of more or less forced elongational flow fields for the stretching operation. That is why, for example, the Sulzer mixer is well–suited for mixing liquids with large differences in viscosity. Moreover, this mixer is more frequently used than the first two, due to its smaller effective pressure drop necessary for a specified increase of the number of striations.

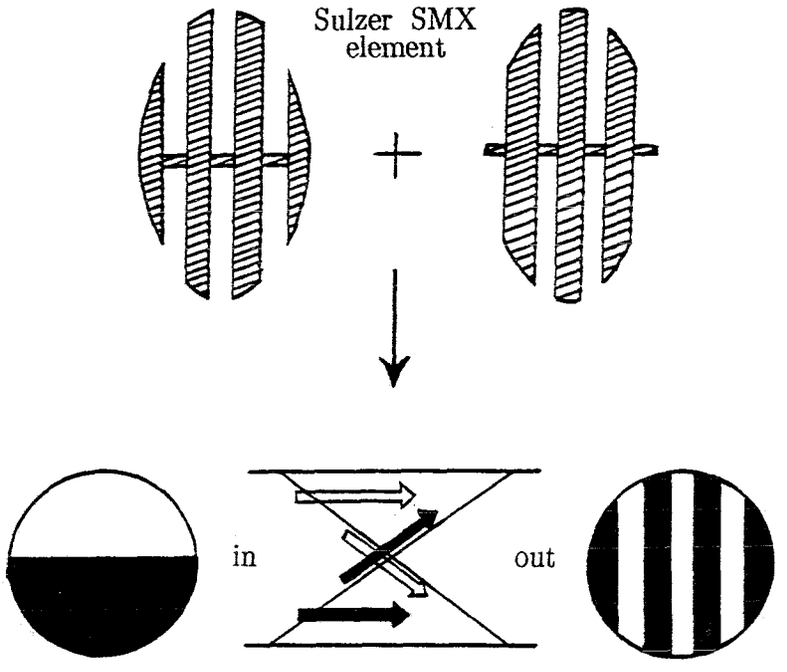

Figure 4.10 *An idea of the Sulzer SMX static mixer, with rather schematical working principle.*

Kenics

The last static mixer to be discussed shortly is the frequently used Kenics mixer, the only one that is based on simple shear for stretching, see Figure 4.11. The elements inside the tube resemble 180^0 twisted platelets, like butterfly ties, with each successive element, again, rotated over 90^0. The working principle is most easily demonstrated if the platelets are thought to be straight, while the relative motion between wall and platelets, during the passage of the flow, is kept the same by adding an imaginary rotation of the barrelwall over the very same 180^0. The approximated drag– and pressure flow inside the cross section of each half of an element are shown in Figure 4.11, as well as the resulting streamlines. Stretching caused by the rotation increases the cross sectional interface typically from 0.5 to 1 tube diameter. Cutting and stacking is cleverly realized by placing the next element under 90^0. Although the Kenics mixer, which yields 2^n layers as readily deduced from its

working principle, shows roughly the same performance in terms of effective pressure drop as the Sulzer mixer, it is not suited for mixing liquids with diverging viscosities since the low viscous material will form sliplayers at the wall, which is fatal for the simple shear based working principle.

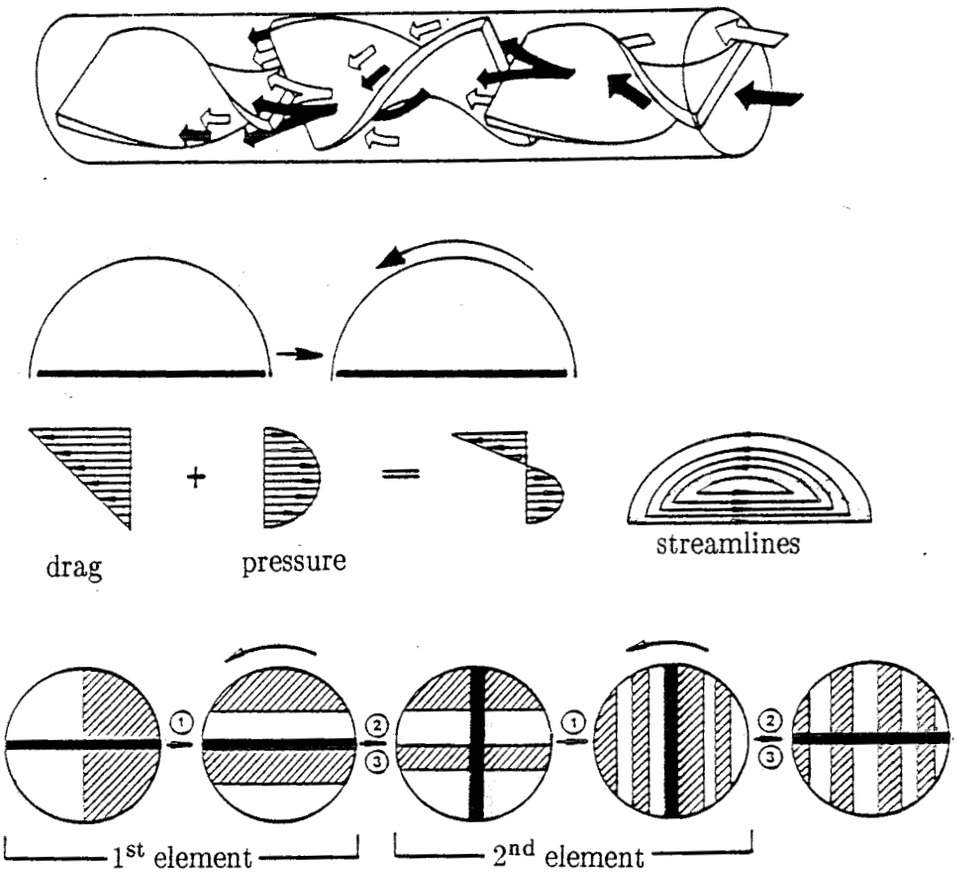

Figure 4.11 *The Kenics static mixer; inside view and idealized working principle.*

4.3.4 Dynamic Mixers

As has been demonstrated in the discussion of static mixers, the principles of efficient distributive mixing can be realized in practice. In operating static mixers, a pressure flow is responsible for the throughput. Consequently, a pressure generating device is needed. Mixing can also be directly improved in these pumps, typically extruders because of their

viscosity independent working principle. This is the area of the dynamic mixers. Although less efficient than in static mixers, also in the continuous flow field of a dynamic mixer stretching, folding, and reorienting can be realized. An illustrative example is the closely intermeshing and, consequently, self wiping corotating twin screw extruder, which induces folds and reorientations with respect to the streamlines during take–over of the material from one screw to the other, see Figure 4.12.

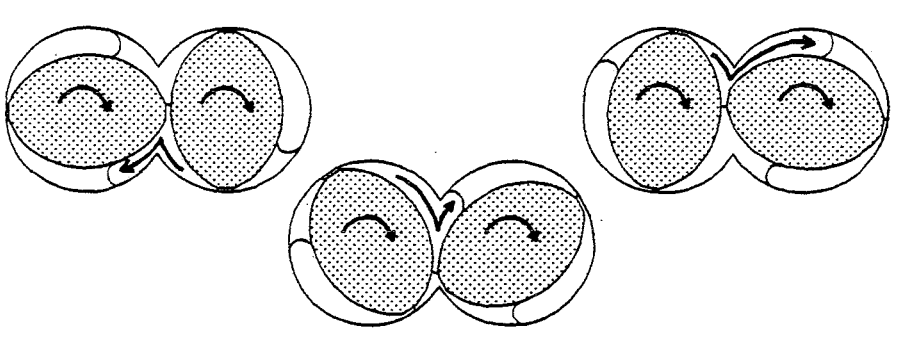

Figure 4.12 *Folding and reorienting in an intermeshing corotating twin screw extruder, during take–over of the material from one screw to the other.*

In contrast to (corotating) twin screw extruders, single screw extruders are inferior mixers, since, despite the helically movement of the flow inside the extruder channel, no reorientation occurs, see e.g. Ottino and Chella (1983, 1985). In order to study the mixing efficiency in extruders, a survey of the different approaches to the modelling can be found in Elemans (1990). Here, it is sufficient to mention that all different mixing elements added to a standard screw – some examples are given in Figure 4.13 – should be designed to induce folds and reorientations. Two specific mixing principles are worthwhile mentioning: (i) The static–dynamic cavity transfer mixer (CTM), which only allows axial transport via a zig–zag type of streamlines, transporting the material from the rotor to different cavities in the stator and from each cavity in the stator back again into all cavities in the rotor. Thus the efficient mixing principle which children apply in the shaking of playing cards is

introduced. (ii) The cokneader, which couples an axial oscillation to a tangential rotation, thus weaving or knitting the material during the axial transport.

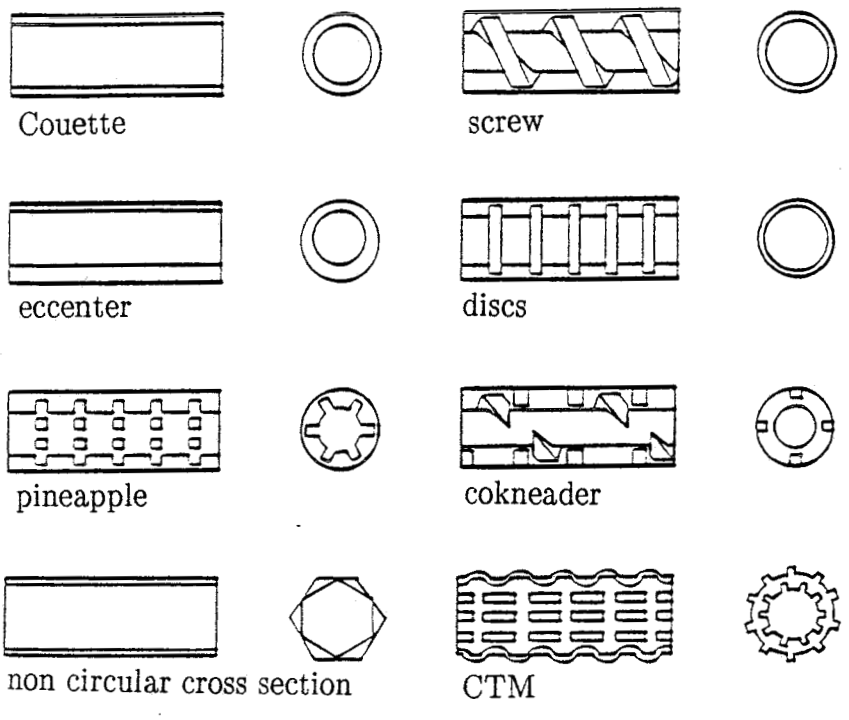

Figure 4.13 *Schematic of various extruder screw elements.*

4.3.5 Continuum Modelling

A systematic approach to the modelling of distributive mixing, valid in general three dimensional flows, is attributed to Ottino's group, publishing a large number of papers on this subject. Of special interest and great didactic value is their numerical and experimental work on periodic (chaotic) flows in 2–D geometries, see e.g. Ottino (1989, 1990). An example of some of their results is shown in Figure 4.14.

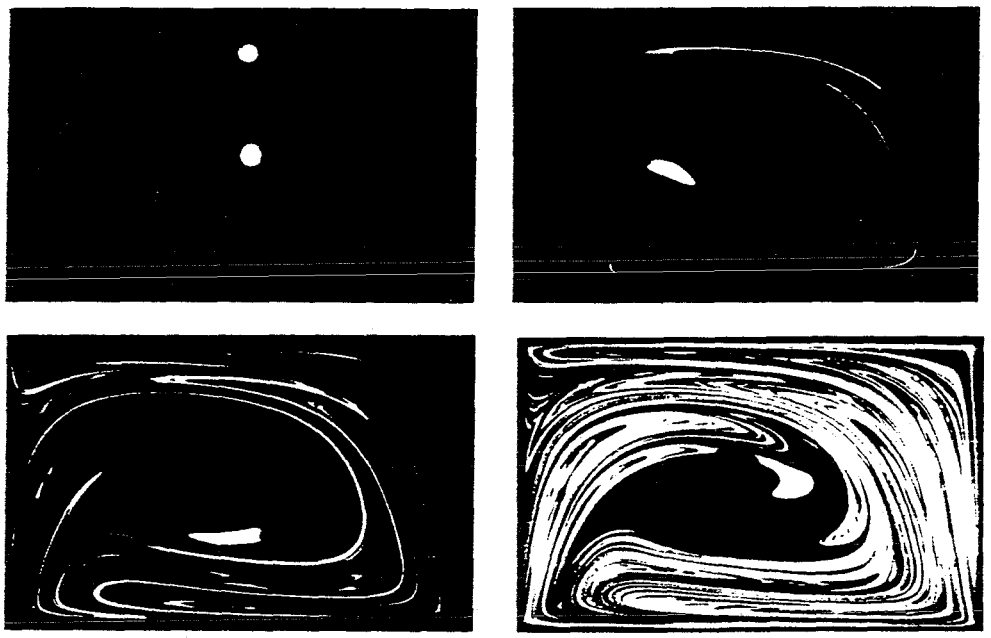

Figure 4.14 *Distributive mixing in a cavity; top and bottom wall are translated periodically (Ottino 1990). Reprinted with permission of Annual Reviews Inc.*

The top and bottom wall of a rectangular duct, a so–called cavity, can be translated independently and periodically. The resulting flow pattern is visualized with two fluorescent tracer drops. No interfacial tension is present between the tracer drops and the continuous phase, so only distributive mixing is studied. In the example of Figure 4.14, one of the blobs is stretched, folded and transferred back to its initial position, before the periodic movement is repeated, thus undergoing efficient mixing (involving horse–shoes). The second blob, however, is only rotated and convected, without any significant deformation. It moves inside a dead zone, called a regular island. The presence or absence of those important zones in general flows, can be analysed by numerical calculation of the local deformation tensor (e.g. the Finger tensor) and multiplication with the blob orientation tensor. Thus the deformation history of 'every particle' can be followed, including folding and reorienting. The importance of folding and reorienting is finally clearly illustrated in Figure 4.15. In these experiments, the tracer was originally placed as a

vertical line in the middle. The resulting deformation patterns are shown for the same total deformation, obtained via a continuous wall movement (Figure 4.15a) and via a discontinuous, periodic movement aimed at the introduction of folds and repetition (Figure 4.15b). The difference between linear and exponential mixing is clearly demonstrated and the results can directly be compared to the working principle of static mixers, see e.g. Figures 4.5 and 4.7.

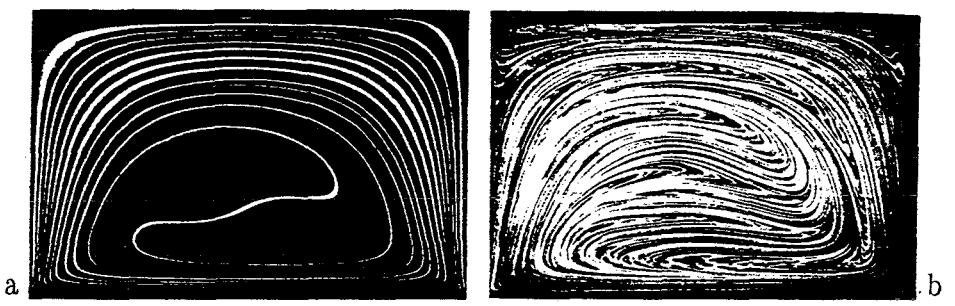

Figure 4.15 *Comparison of a) continuous and b) discontinuous movement of the cavity walls; the total displacement of the walls is equal in both cases (Leong and Ottino 1989). Reprinted with permission of Cambridge University Press.*

Mathematically, the prerequisites for these so–called chaotic flows are known (implying the introduction of horse–shoes in the flow), see Ottino (1989, 1990). Therefore, in principle three dimensional continuous mixers can be designed according to optimal principles of mixing. Also existing designs can be analysed with respect to the occurence of regular islands, which should be avoided anyway, and to the chaotic character of the flow, which should be incorporated. Even in 2–D geometries, the computing time could be excessive. Nevertheless, this rigorous approach yields the most systematic route to most of the mixing problems met in polymer processing and chemical technology, but also in geology, oceanography, or air pollution, since apart from multiphase flows also diffusion and chemical reaction can be incorporated straightforwardly in this concept, see Paragraph 4.4.8 (Ottino 1991).

4.4. Dispersive Mixing ($Ca \approx Ca_{crit}$)

4.4.1 Rayleigh Disturbances

When the original millimeter sized liquid drops are extended into long slender filaments, due to the affine deformation, local radii are decreased such that the interfacial tension starts playing a role (active interfaces). In polymer melts, the shear stress and the interfacial stress become of the same order of magnitude if the radius (R) of the threads is decreased to 1 μm:

$$\left.\begin{aligned} \tau &= \eta_c \dot{\gamma} = 10^2 \cdot 10^2 = 10^4 \text{ Pa} \\ \sigma/R &= 10^{-2} \,/\, 10^{-6} = 10^4 \text{ Pa} \end{aligned}\right\} \quad Ca = \frac{\eta_c \dot{\gamma} R}{\sigma} = 1 \qquad (4.21)$$

The interfacial tension tends to minimize the interface between the two phases, minimizing the surface to volume ratio. As a consequence, small disturbances present at the interface of the liquid cylinder grow and finally result in the disintegration of the thread into a line of drops. These so–called Rayleigh disturbances can be investigated experimentally every morning in the shower and are illustrated for a molten Polyamide–6 (PA–6) filament, in an otherwise quiescent melt of PS, in Figure 4.16. It should be noted that a major difference between the two processes indicated is the value of the Reynolds number. In the shower the interfacial stress mainly compares to inertia (We_1), see Weber (1931), while in molten polymer blends it compares to viscous shear stresses (Ca); see Equations 4.1–4.4.

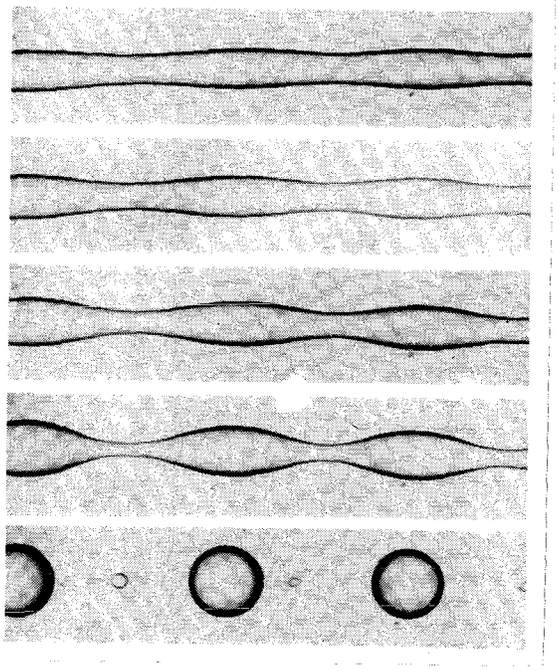

Figure 4.16 *Disintegration of a PA−6 thread (diameter 55 μm) in a quiescent PS matrix at 230°C (Elemans et al. 1990), see also Figure 4.A.1. Reprinted with permission of the Society of Rheology.*

Since in Figure 4.16 the viscosities are high and the thread is relatively thick, implying a small driving force (σ/R), the timescale of the experiment is typically minutes in comparison with the timescale of seconds in the free water jets breakup. Inbetween the drops, small satellite droplets are formed in the last stage of the disintegration process, due to fast growth of Rayleigh disturbances on the fine filaments (σ/R large) formed between adjacent drops. Tjahjadi et al. (1992) numerically investigated the formation of satellite and sub–satellite droplets and found that the smaller the viscosity ratio p between thread and matrix, the more satellite droplets are formed.

Figure 4.17 explains that only disturbances with a wavelength larger than the circumference of the original thread ($\lambda > 2\pi R_0$) result in a monotonic decrease of the interfacial area with an increase of the amplitude. Disturbances with a smaller wavelength, initially result in an increase of the interfacial area and therefore damp and extinguish.

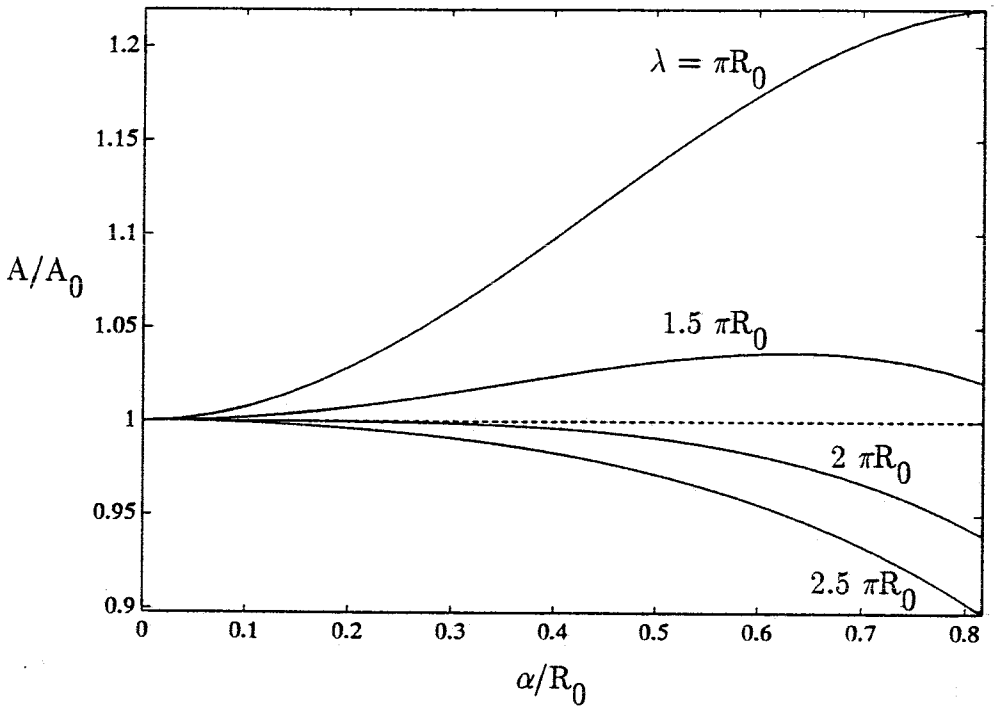

Figure 4.17 *Relative interfacial area of a sinusoidally disturbed cylinder versus the relative amplitude α/R_0 of disturbance, for different wavelengths. The interfacial area monotonically decreases if $\lambda > 2\pi R_0$.*

4.4.2 Disintegration of Threads at Rest

Classical theories exist for the mathematical description of the disintegration of a Newtonian thread embedded in a quiescent, Newtonian continuous phase, with neglect of inertia, see Rayleigh (1879) and Tomotika (1935).

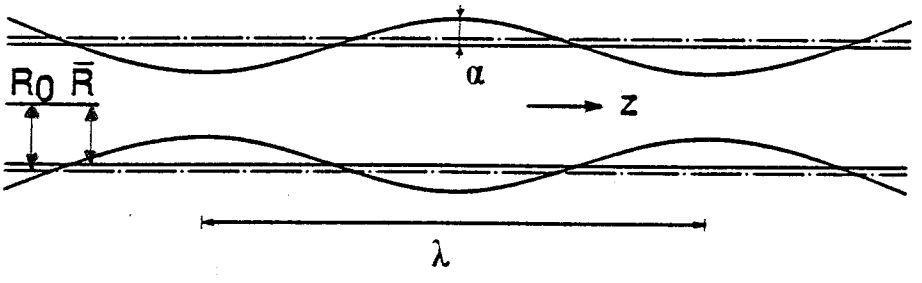

Figure 4.18 *Sinusoidal Rayleigh disturbance on a liquid cylinder.*

Figure 4.18 shows a sinusoidal Rayleigh disturbance on a liquid cylinder with radius:

$$R(z) = \overline{R} + \alpha \sin\left[\frac{2\pi z}{\lambda}\right] \tag{4.22}$$

where the average radius equals:

$$\overline{R} = \sqrt{R_0^2 - \alpha^2/2} \tag{4.23}$$

The disturbance amplitude α [m] grows exponentially in time:

$$\alpha = \alpha_0 e^{qt} \tag{4.24}$$

with growth rate q [s^{-1}]:

$$q = \frac{\sigma \Omega(\lambda_m, p)}{2\eta_c R_0} \tag{4.25}$$

where

α_0 = original disturbance amplitude [m]

R_0 = radius of the undisturbed thread [m]

Ω is the dimensionless growth rate of the disturbance, a function of the viscosity ratio p and the wavelength λ (Tomotika 1935, Chappelear 1964, Palierne and Lequeux 1991). In the beginning, small amplitudes of, in principle, all wavelengths are present. For a given value of p, however, only one disturbance with the dominant wavelength (λ_m) grows fastest and finally results in disintegration of the thread. Figure 4.19 shows the dominant

wavenumber X_m ($= 2\pi R_0/\lambda_m$) and the corresponding dimensionless growth rate Ω_m as a function of p.

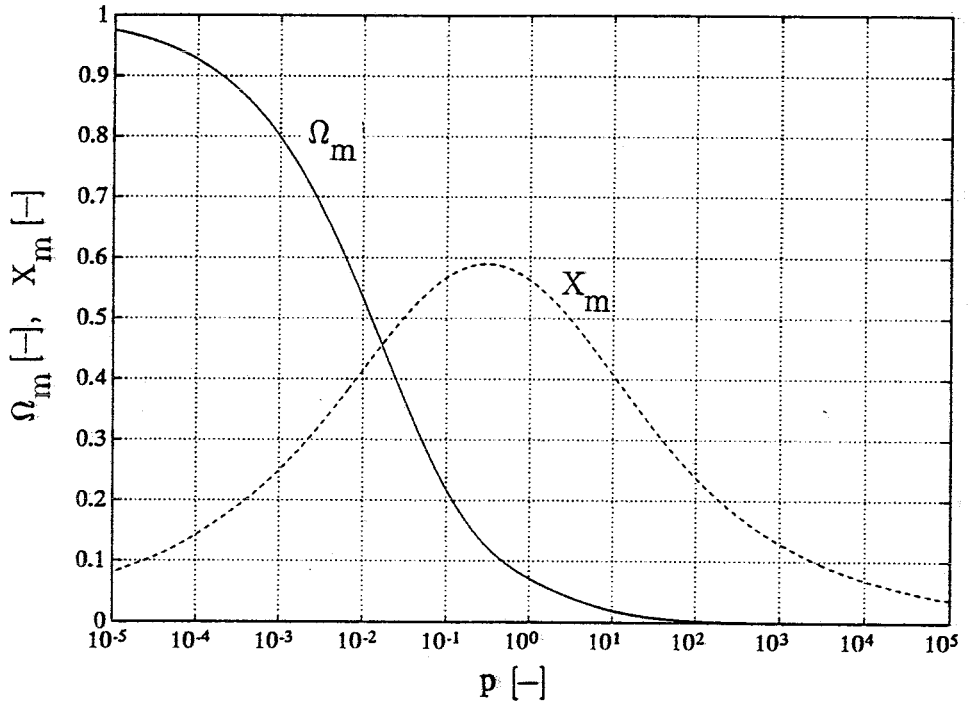

Figure 4.19 *Dominant wavenumber X_m ($= 2\pi R_0/\lambda_m$) and corresponding growth rate Ω_m of interfacial disturbances versus viscosity ratio p ($= \eta_d/\eta_c$).*

The time required for breakup can be calculated from Equation 4.24:

$$t_b = \frac{1}{q} \ln (\alpha_b/\alpha_0) \qquad (4.26)$$

where α_b is the amplitude at breakup. Breakup occurs when the amplitude equals the average radius of the thread $\overline{R}$, yielding the amplitude α_b:

$$\alpha_b = \sqrt{2/3} \cdot R_0 \approx 0.82\ R_0 \qquad (4.27)$$

Kuhn (1953) proposed an estimation of the initial amplitude α_0, based on temperature fluctuations due to Brownian motion. With T the absolute temperature and k Boltzmann's constant ($1.4 \cdot 10^{-23}$ J/K), he derived:

$$\alpha_0 = \sqrt{\frac{21kT}{8\pi^{3/2}\sigma}} \tag{4.28}$$

Combination of Equations 4.25–4.28 results in:

$$t_b = \frac{\eta_c R_0}{\sigma \Omega_m} \ln (10^{23} \sigma R_0^2 / T) \tag{4.29}$$

From Equations 4.25 and 4.29 it can be seen that the characteristic timescale for the σ–driven development of interfacial disturbances is $t_\sigma = \eta_c R_0 / \sigma$ and time can be non–dimensionalized:

$$t^* = t \frac{\sigma}{\eta_c R_0} \tag{4.30}$$

thus:

$$t_b^* = \frac{1}{\Omega_m} \ln (10^{23} \sigma R_0^2 / T) \tag{4.31}$$

Please note that some authors (Stone and Leal 1989 a,b; Tjahjadi and Ottino 1991) multiply η_c in t_σ by (1+p), which is equivalent to a substitution of η_c by $(\eta_c+\eta_d)$, in order to incorporate the effect of the viscosity ratio in the dimensionless timescale. The estimation of the initial amplitude α_0 by Kuhn (1953) yields values of about 10^{-9} m that are somewhat

arbitrary. Mikami et al. (1975) suggest α_0 to be 10^{-8} to 10^{-7} m; in that case, of course, Equation 4.26 should be used rather than 4.29 or 4.31.

For incompressible liquids, the diameter 'a' of the newly formed droplets can be obtained from the conservation of mass (or volume):

$$a = R_0 \sqrt[3]{12\pi/X_m} \qquad (4.32)$$

For instance, given the viscosity ratio p = 1, $X_m = 0.56$ (see Figure 4.19) and the diameter of the new droplets equals twice that of the original thread.

The theory outlined above applies to Newtonian liquids at rest. In case the thread is viscoelastic, orientational stresses build up during formation of the thread, provided that the Deborah number $De = \theta/t_G \geq O(1)$, where θ is the relaxation time of the fluid and t_G the timescale of the flow. If these stresses relax slower than the growth rate of interfacial disturbances, i.e. $De = \theta/t_\sigma \geq O(1)$, the drainage of the filaments into the developing drops (extensional flow) is retarded due to the increased extensional viscosity. Typical dumbbell shapes develop (Figure 4.20b) rather than sinusoids (Figure 4.20a) and the growth of the disturbances almost stagnates. Consequently, the resulting breakup time is larger than in the equivalent Newtonian case. The theory for Newtonian liquids sometimes proves to be useful even for molten polymers, as evidently shown by the sinusoidal disturbances on the polymer thread in Figure 4.16. The diameter of the thread in this model experiment is relatively thick as compared to the typical microfibers formed in the dynamic mixing process in extruders and, consequently, the timescale to breakup is large. An application of this theory to measure the interfacial tension in molten polymer systems is discussed in Appendix 4.A.

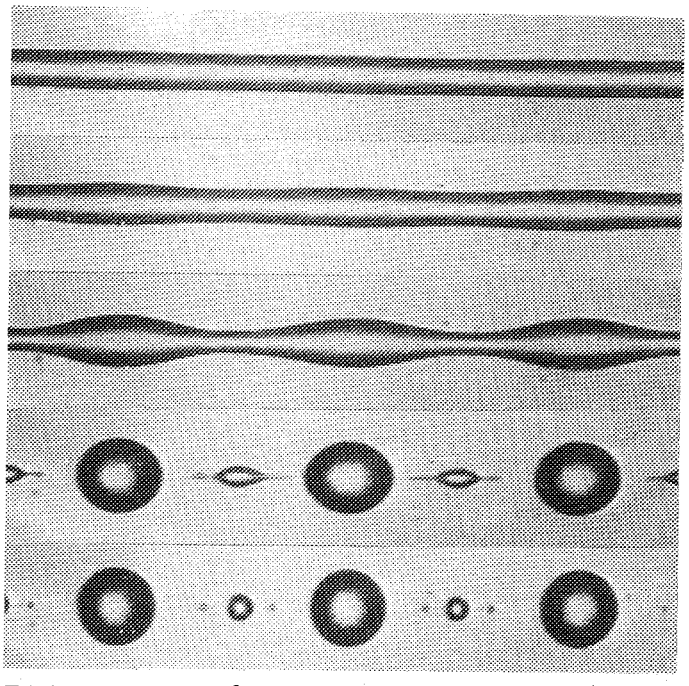

Figure 4.20 a *Disintegration of a 0.35 mm Newtonian thread (castor oil, $\eta_d \approx 0.7$ Pa.s) in a quiescent Newtonian matrix (silicon oil, $\eta = 0.9$ Pa.s, $\sigma = 0.004$ N/m) at roomtemperature; successive photographs after every second.*

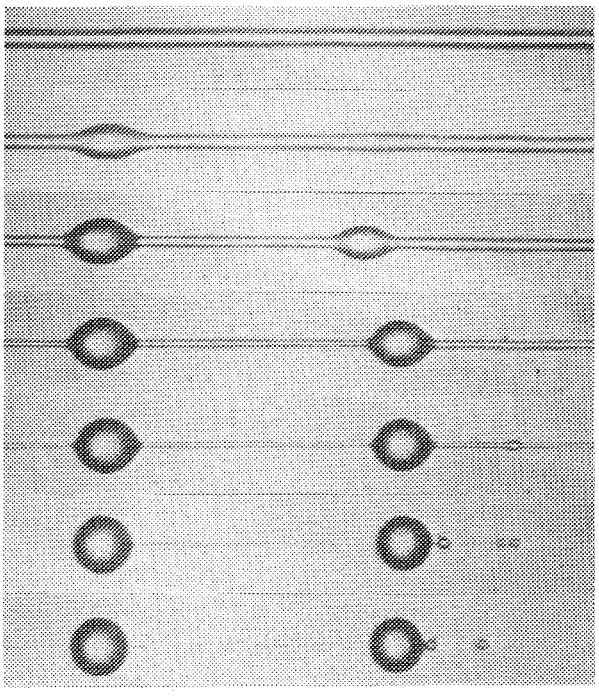

Figure 4.20 b *Disintegration of a 0.07 mm viscoelastic thread (80% corn syrup/ 20% water/ 0.01% polyacrylamide, $\eta_d \approx 0.5$ Pa.s, $\theta \approx 10$ s) in a quiescent Newtonian matrix (silicon oil, $\eta = 2$ Pa.s, $\sigma = 0.025$ N/m) at roomtemperature; successive photographs after every 3 seconds.*

4.4.3 Disintegration of Threads during Flow

In a flowing medium, breakup of threads is delayed, since the extension of a thread causes an increasing wavelength of the disturbances in combination with a decreasing thread diameter. Consequently, the initially dominant wavenumber $X_m(0) = 2\pi R_0(0)/\lambda_m(0)$ decreases continuously in time. It will not represent the fastest growing disturbance during all distinct time steps and eventually can damp and become extinct. A new disturbance, with wavenumber $X_m(t) = 2\pi R_0(t)/\lambda_m(t)$, grows faster and will become dominant despite of its start with a smaller amplitude. On any moment, a particular wavenumber $X_m(t)$ is dominant and grows fastest; disturbances continuously grow and damp. In the end, the amplitude of one disturbance equals the time dependent average radius of the thread and causes disintegration of the thread, see Figure 4.21.

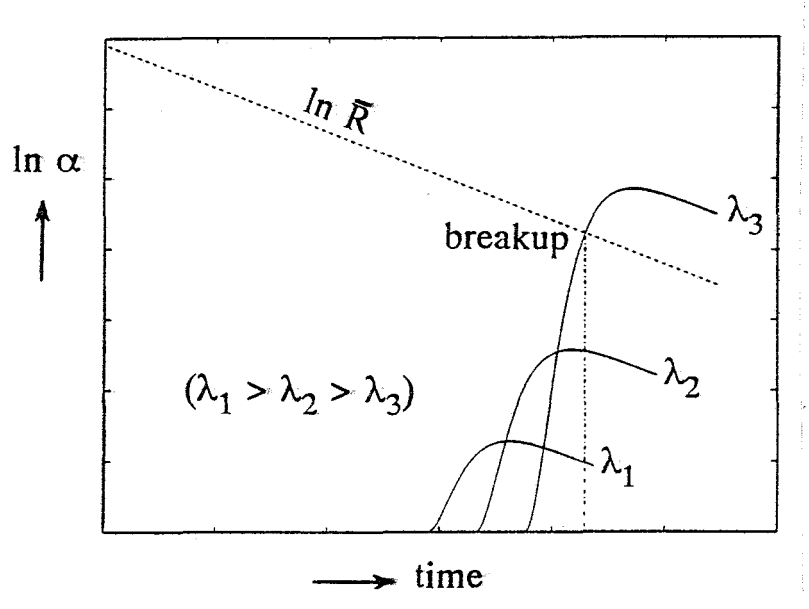

Figure 4.21 *Progress of the average radius $\overline{R}$ of a thread – which is extending at a uniform rate – and of the amplitude α of disturbances with different initial wavelengths.*

More time till breakup is required if this external flow field is present since the flow stabilizes the thread morphology and allows a further decrease in thread diameter; a finer dropletsize will result. A number of researchers investigated this practically important phenomenon, for Newtonian liquids only, (Tomotika 1936, Mikami et al. 1975, Khakhar and Ottino 1987, Tjahjadi and Ottino 1991). The analysis is based on affine extension of the thread which maintains a circular cross section. No simple explicit equations result and Figure 4.22 was calculated to give access to the results of the analysis.

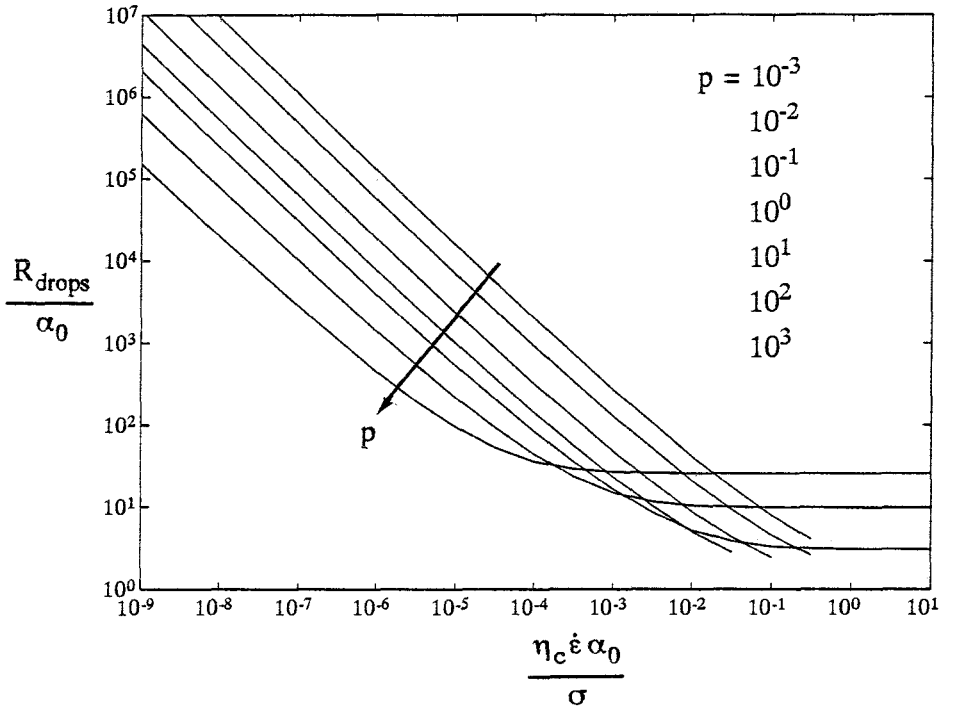

Figure 4.22 *Dimensionless drop radius resulting from disintegration of a Newtonian liquid thread which is extending at a uniform rate $\dot{\epsilon}$.*

Upon an increase of the extension rate of the thread, smaller droplets result from the disintegration process. The extension rate $\dot{\epsilon}$ can be defined formally in any type of flow: clearly in extensional flows but also in simple shear flow where $\dot{\epsilon}$ is in principle time dependent because of variation in time of the thread orientation. Since both quantities (R_{drops} and $\dot{\epsilon}$) are presented in dimensionless form, the curves in Figure 4.22 hold for any

realistic range of material parameters and processing conditions. The different curves correspond to different viscosity ratios p. For low enough values of the dimensionless parameter $\eta_c \dot{\epsilon} \alpha_0 / \sigma$ a larger p yields smaller droplets, since disturbances grow more slowly on a highly viscous thread (compare Ω_m for a thread at rest, Figure 4.19). In other situations, the optimal value of p for obtaining the smallest final dropsize depends on the value of $\eta_c \dot{\epsilon} \alpha_0 / \sigma$ that can be realized in practice.

Note that the initial radius of the thread has no effect on the resulting dropsize, although it evidently determines the breakup time. The time for breakup can be roughly approximated from the affine deformation of the extending thread, starting with the initial drop radius and ending with R_{drops}. *As mentioned in the previous paragraph, the value of* α_0 *is, unfortunately, quite arbitrary (*10^{-8} *m seems reasonable), thus absolute predictions of the minimum attainable dropsizes still deal with some uncertainties. A physical lowerlimit for the dropsize arises from the fact that the average thread radius cannot decrease below* α_0. *As indicated in Paragraph 4.4.2, viscoelasticity of the thread will have a pronounced influence on these transient processes, if the relevant Deborah numbers are of order unity. This aspect is still under investigation in our laboratory.*

4.4.4 Experimental Devices

After affine deformation, at Ca >> Ca_{crit}, and disintegration of the threads formed, into lines of droplets, finally these droplets are subjected to deformation caused by the flow field. Since now Ca ≈ Ca_{crit}, breakup will depend upon the strength of the flow field and the viscosity ratio p. This is the classical subject of study in dispersive mixing and excellent reviews are given by Acrivos (1983) and Rallison (1984). Experimentally, drops (∼ 1 mm) of low viscous (non–)Newtonian model liquids are injected at roomtemperature in a well–defined shear field, like simple shear between two infinite bands or in a Couette

device (see Figure 4.23) and elongational flow in a four roll mill (see e.g. Taylor 1934, Grace 1971, Bentley 1986 a,b, Stone and Leal 1989 a,b, Meijer and Bos 1989, Elemans 1989, de Bruin 1989).

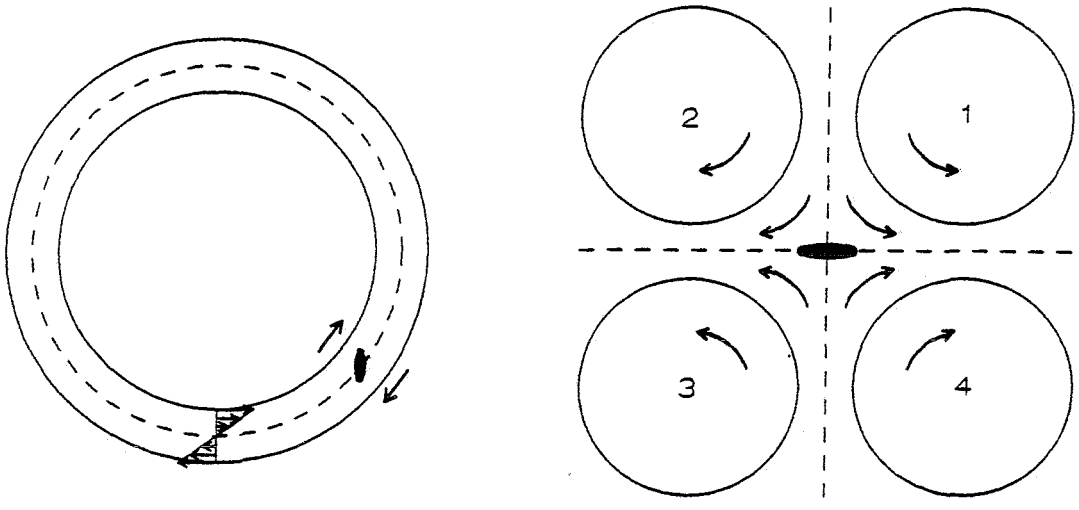

Figure 4.23 *The Couette device (simple shear flow) and the four roll mill (2–D elongational flow).*

In our laboratory, recently a computer controlled opposed jets device was developed, (Janssen et al. 1991), to study the transient deformation and breakup of viscoelastic drops, see Figure 4.24. It consists of four solid blocks, fixed between two parallel plates. From two opposite directions, the continuous phase is pumped into the cell, yielding a stagnation flow which is very similar to the flow field in the four roll mill, at least in a region near the centre of the cell.

The main difference as compared to the four roll mill is the separation of functions realized by this flow: (i) The deformation rate is set by the overall flow rate through the cell. (ii) The type of flow (see also Paragraph 4.4.5) is determined by the shape of the four blocks, and, finally: (iii) The control of the, principally unstable, position of the deforming drop at the stagnation point is carried out by a computer controlled variation of the ratio of both

exit flow rates (by a small rotation of a valvesystem mounted between exit channels and reservoir) thus shifting the actual position of the stagnation point just beyond the displaced drop. The control mechanism developed, proves to be fast and efficient, i.e. within displacements of the drop of only one pixel of the digitized image. In the four roll mill all three functions are carried out by varying the individual roller speeds, yielding a complex control strategy (Bentley and Leal 1986 a). The four roll mill is flexible, however, since a variation of the type of flow is possible even within one experiment. The opposed jets device is small, on the contrary, the inner cell dimensions are only a few centimeters without experiencing problems with unwanted wall effects, as followed from numerical simulations of the internal flow field and confirmed by laser Doppler anemometry of the real 3–D velocity profile. Since the cell is small and can be designed as a closed loop, the system is accessible for research to polymer melts at elevated temperature as well.

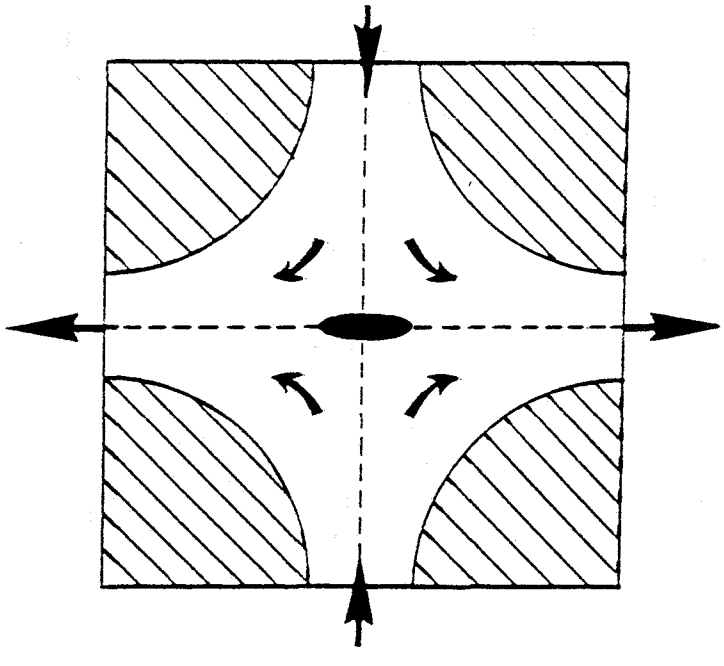

Figure 4.24 *The opposed jets device: in a fixed geometry two liquid jets are forced to collide, resulting in an elongational flow in the stagnation point (Janssen et al. 1991).*

4.4.5 Flow Classification

Before turning to the experiments on drop deformation and breakup, it is useful to shortly discuss the classification of different types of flow, after Giesekus (1962), Tanner (1976), Fuller and Leal (1981) or Olbricht et al. (1982). A general class of experimentally and numerically accessible flows is that of the linear 2–D flows given by:

$$\vec{u} \quad = \quad (\vec{\nabla}\vec{u})^{c} \cdot \vec{x} \; = \; \mathbf{L} \cdot \vec{x} \tag{4.33}$$

with $\vec{u}$ the velocity vector, $\vec{\nabla}$ the gradient operator, $\vec{x}$ the position vector, and $\mathbf{L}$ the velocity gradient tensor:

$$\mathbf{L} \quad = \quad \frac{G}{2}\begin{bmatrix} 1+\alpha & 1-\alpha & 0 \\ -1+\alpha & -1-\alpha & 0 \\ 0 & 0 & 0 \end{bmatrix} \qquad \text{with} \qquad -1 \leq \alpha \leq 1 \tag{4.34}$$

In Cartesian coordinates $\vec{x}$ (x,y,z) the velocity components of $\vec{u}$ (u,v,w) are respectively:

$$\begin{aligned} u \quad &= \quad \frac{G}{2}\Big[\, (1+\alpha)x \; + \; (1-\alpha)y \,\Big] \\ v \quad &= \quad \frac{G}{2}\Big[(-1+\alpha)x + (-1-\alpha)y\Big] \\ w \quad &= \quad 0 \end{aligned} \tag{4.35}$$

G (s^{-1}) is the (scalar) velocity gradient and the type of flow is characterized with one single parameter α. In Figure 4.25 streamlines are shown for various values of α yielding as many specific types of flow.

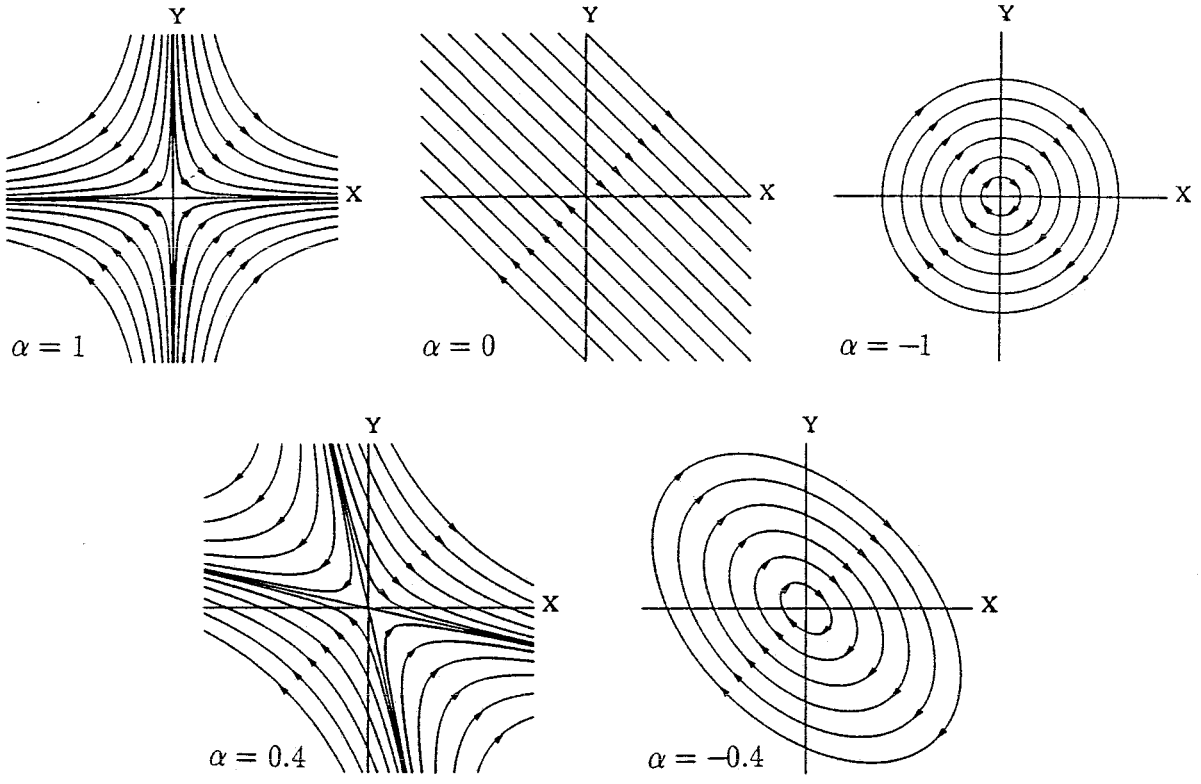

Figure 4.25 *Streamlines of some specific linear 2–D flows: $\alpha = 1$ plane hyperbolic flow; $\alpha = 0$ simple shear flow; $\alpha = -1$ pure rotational flow.*

$\alpha = 1$ the velocity components are: u = Gx, v = –Gy, w = 0.
This represents plane hyperbolic or 2–D elongational flow, G is usually denoted $\dot{\epsilon}$.

$\alpha = 0$ the velocity components are better defined relatively to a basis which is rotated over 45°: u' = Gy', v' = 0, w' = 0.
This is simple shear flow, G is usually denoted $\dot{\gamma}$.

$\alpha = -1$ the velocity components read: u = Gy, v = –Gx, w = 0.
This represents pure rotational flow.

Values of α inbetween these extremes yield combined flows. As usual, **L** is split into a symmetric part **D** and a skew–symmetric part **Ω**:

$$\mathbf{L} = \mathbf{D} + \mathbf{\Omega} \tag{4.36}$$

with **D** the rate of deformation tensor:

$$\mathbf{D} = \frac{1}{2}(\mathbf{L} + \mathbf{L}^{c}) = \frac{G}{2}\begin{bmatrix} 1+\alpha & 0 & 0 \\ 0 & -1-\alpha & 0 \\ 0 & 0 & 0 \end{bmatrix} \tag{4.37}$$

and $\mathbf{\Omega}$ the spintensor:

$$\mathbf{\Omega} = \frac{1}{2}(\mathbf{L} - \mathbf{L}^{c}) = \frac{G}{2}\begin{bmatrix} 0 & 1-\alpha & 0 \\ -1+\alpha & 0 & 0 \\ 0 & 0 & 0 \end{bmatrix} \tag{4.38}$$

Plane hyperbolic flow ($\alpha = 1$) is free of rotation ($\mathbf{\Omega} = 0$) and therefore called strong in deformation, while in pure rotational flow ($\alpha = -1$) no deformation results ($\mathbf{D} = 0$). Simple shear flow ($\alpha = 0$) shows both contributions.

In order to be able to define a Capillary number in all these types of flow, it is consistent to use a scalar value for the shear rate, obtained for pure deformation, consequently after substraction of rigid rotation. Using the definition:

$$\dot{\gamma} = \sqrt{2\mathbf{D}:\mathbf{D}} \tag{4.39}$$

the rotational components of **L** are eliminated. Using Equation 4.39, the Capillary number now may be uniquely defined for Newtonian systems:

$$\mathrm{Ca} = \frac{\eta_c \dot{\gamma} R}{\sigma} \tag{4.40}$$

In the definitions for Ca and p, only shear viscosities are used. With help of Equation 4.39, the shear rate $\dot{\gamma}$ can be defined in any linear 2–D flow (given by Equations 4.33–4.34) from pure rotational to irrotational elongational flow:

$$\dot{\gamma} = (1+\alpha)\,G \tag{4.41}$$

Definition 4.39 is calibrated for simple shear flow where the shear rate $\dot{\gamma}$ must equal the velocity gradient G. In plane hyperbolic flow ($\alpha = 1$) apparently $\dot{\gamma} = 2G\ (= 2\dot{\epsilon})$, while for pure rotational flow ($\alpha = -1$) the Capillary number becomes zero as it should, since no shear stress can be applied on the drop: $\dot{\gamma} = 0$. Summarizing:

$$Ca = \frac{\eta_c 2GR}{\sigma} \qquad \text{in hyperbolic flow} \tag{4.42}$$

$$Ca = \frac{\eta_c GR}{\sigma} \qquad \text{in simple shear flow} \tag{4.43}$$

$$Ca = \frac{\eta_c 0R}{\sigma} = 0 \qquad \text{in rotational flow} \tag{4.44}$$

To exert the same Capillary number on a drop, the shear rate in simple shear flow must be twice the elongation rate in 2–D elongational flow. Note that this does not originate from a faulty modified Trouton ratio but is simply due to the fact that in simple shear half of the rate of deformation is used for rotation, while in elongational flow it is completely used for effective deformation. As a consequence, especially the flows with $0 < \alpha \leq 1$, the so–called strong flows, are of interest for dispersive mixing.

The definitions of $\dot{\gamma}$ and Ca, given here, are in accordance with those used by Taylor (1934), Grace (1971), and Ottino (1991). The group of Leal substitutes just the velocity gradient G in the Capillary number, instead of $\dot{\gamma}$ (= (1+α)G), yielding a difference of a factor 2 in Ca for all results on 2–D elongational flow.

As a final example, a linear 3–D axisymmetric elongational flow is considered, defined with velocity gradient tensor:

$$\mathbf{L} = \frac{G}{2}\begin{bmatrix} 2 & 0 & 0 \\ 0 & -1 & 0 \\ 0 & 0 & -1 \end{bmatrix} \tag{4.45}$$

consequently u = Gx, v = $-\frac{G}{2}$ y, and w = $-\frac{G}{2}$ z. Like in 2–D elongational flow, also here $\mathbf{D} = \mathbf{L}$ and $\mathbf{\Omega} = \mathbf{0}$, the flow is free of rotation. According to Equation 4.39 the shear rate equals $\dot{\gamma} = G\sqrt{3}$. Because of rotational symmetry, this flow is often used in numerical studies. It can be realized by suction of fluid from the area between two trumpet shaped dies.

4.4.6 Experiments on Drop Deformation

The most extensive experimental study originates from Grace (1971). He determined the critical Capillary number, in more or less equilibrium situations by slowly increasing the velocity gradient G, in simple shear and elongational flow, until no more stable drop shape could be obtained. Below Ca_{crit}, the interfacial tension dominates and the drop will slightly deform but not breakup; a typical internal circulation flow maintains a stable equilibrium drop shape. Just above Ca_{crit}, no stable drop shape exists, the shear stress dominates and, after some time, leads to breakup. In Figure 4.26 Grace's results are summarized.

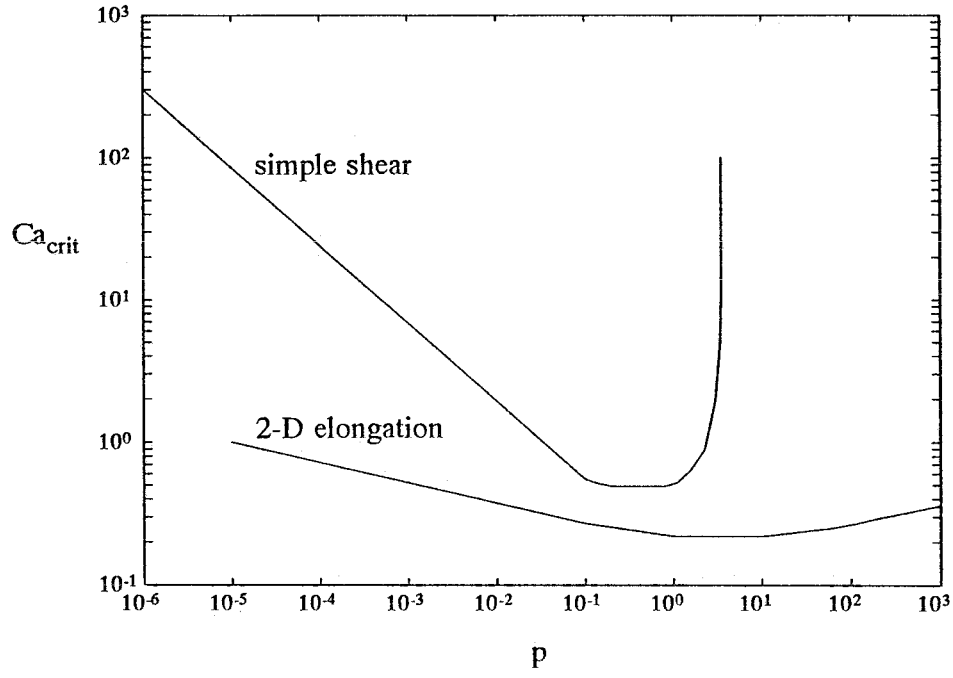

Figure 4.26 *Critical Capillary number versus viscosity ratio p ($= \eta_d/\eta_c$), in simple shear and in elongational flow (after Grace 1971).*

As for distributive mixing, also for dispersive mixing elongational flow is more efficient than simple shear flow, especially for p > 4, where the absence of rotational components in elongational flow still leads to breakup. Independent of the type of flow, the minimum value of Ca_{crit} is found around p = 1.

This does not necessarily imply that always at p = 1 the smallest droplets can be obtained, since in a dynamic mixing process small droplets are not formed by successive breakup at Ca_{crit}. Rather than formed under equilibrium conditions, small droplets originate from a large drop extended by the flow into a thin thread, stabilized by the same flow, that finally disintegrates at once into a row of small droplets, as described in Paragraph 4.4.3. Figure 4.27 compares the dropsizes generated by the two distinct processes. The full curves originate from Figure 4.22. The dashed curves were based on Grace's values of the critical Capillary number (for plane hyperbolic flow) from which a minimum attainable dropsize

can be calculated for given values of $\eta_c \dot{\epsilon}/\sigma$ and p. It is evident that in the dynamic process, p = 1 is not generally the optimum viscosity ratio. If droplets have been formed by the dynamic process while the quasi equilibrium process would result in smaller droplets (typically at high values of $\eta_c \dot{\epsilon}/\sigma$), they just break once more. In a practical situation, an extra point to consider is whether the time for each of the processes is sufficiently large. In the dynamic process the time for breakup is mainly determined by affine deformation. In the quasi equilibrium process the time for breakup was measured by Grace (1971), as discussed later in this paragraph.

The dashed curves in Figure 4.27 can be calculated for dropsizes down to irrealistic small scales. Of course, the dropsize is limited by a lengthscale (~ 10^{-9} m) below which continuum mechanics cannot be applied. Changing the arbitrary value of α_0 (10^{-8} in the figure) has the effect of shifting the (full) curves of the dynamic process along the -45^0 diagonal. The value of $\eta_c \dot{\epsilon}/\sigma$ typically ranges from 1 to 10^5 m^{-1} for model liquids in an experimental device (e.g. opposed jets, four roll mill, or Couette) and from 10^4 to 10^8 m^{-1} for polymer melts in an extruder.

Figure 4.28 illustrates the deformation and breakup of a Newtonian drop in simple shear flow at Ca just above Ca_{crit}. From preliminary experiments in the opposed jets device it has become clear that moderate viscoelasticity of the drop affects Ca_{crit} only slightly (see also Milliken and Leal 1991, 1992).

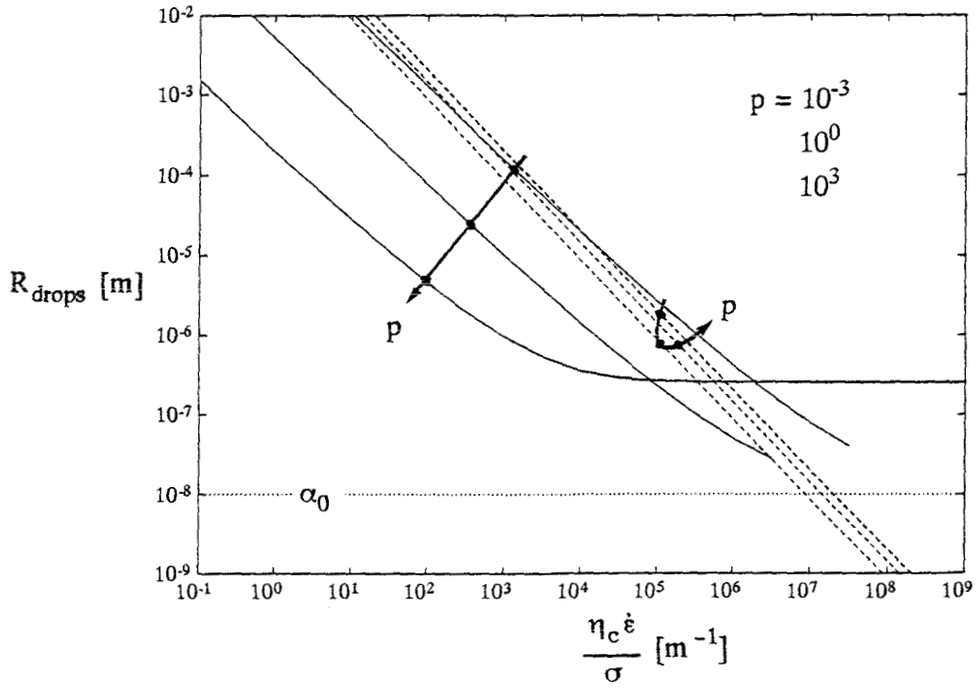

Figure 4.27 *Minimal attainable dropsize resulting from (i) the dynamic process of thread breakup during extension, with $\alpha_0 = 10^{-8}$ m (full curves) and (ii) quasi equilibrium drop breakup at Ca_{crit} in 2–D extension (dashed curves). Parameter is the viscosity ratio p.*

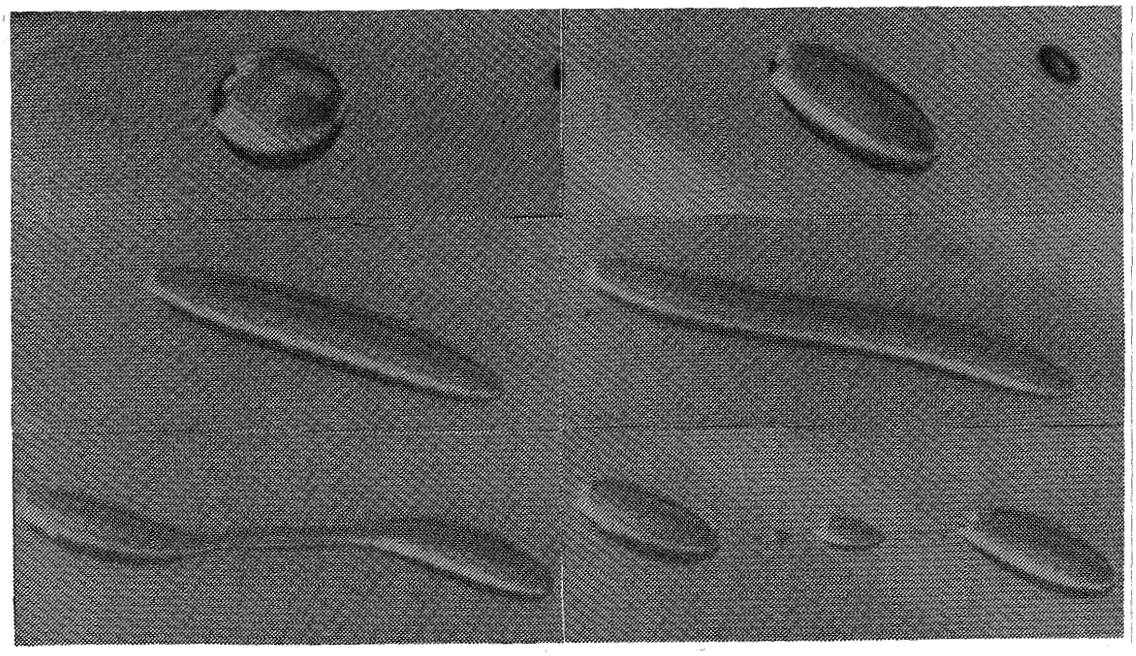

Figure 4.28 *Breakup of a drop (~ 1 mm) in simple shear flow just above the critical Capillary number (Newtonian model liquids, p = 0.14).*

Depending on the viscosity ratio p, Rumscheidt and Mason (1961) distinguish four classes of deformation and breakup in simple shear flow. For $p > 1$ the deformed drop has rounded ends while for smaller p these become pointed. If $p < 0.1$ extremely small droplets break off from the sharply pointed ends. This phenomenon, called tipstreaming, is caused by gradients in the interfacial tension due to convection of surfactants along the drop surface. At the tips the interfacial tension is locally lowered so that tiny droplets break off (de Bruijn 1991).

As already stressed, it is important to focus on the dynamics of the process and the time necessary for deformation and breakup. This was measured by Grace and his results, again obtained under quasi equilibrium conditions, are given in Figure 4.29. The dimensionless breakup time t_b^* proves to be strongly dependent on p.

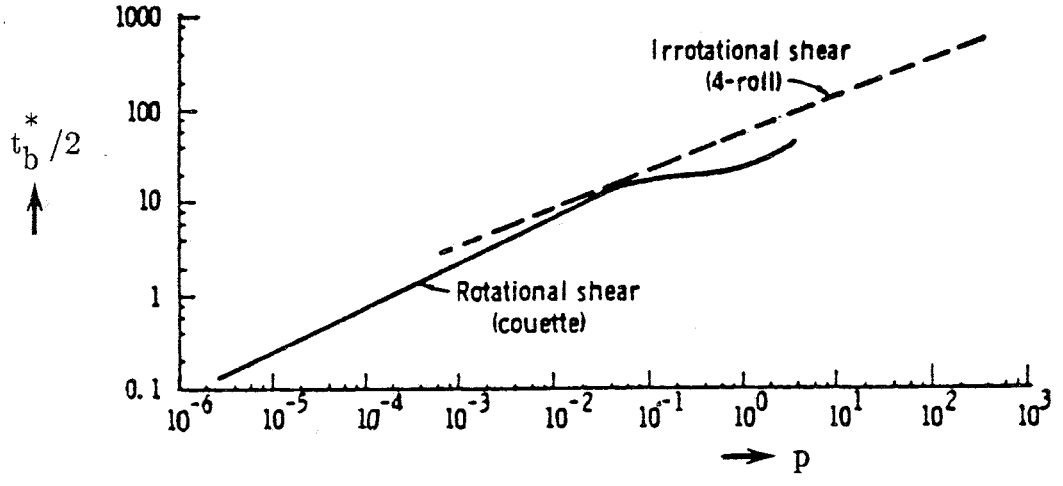

Figure 4.29 *Dimensionless time (Equation 4.30) for drop breakup at Ca slightly above Ca_{crit} as a function of the viscosity ratio (Grace 1971). Reprinted with permission of Gordon and Breach Science Publishers Inc.*

Upon exceeding Ca_{crit} in simple shear flow, the breakup time decreases, according to Grace, see Figure 4.30. However, these experimental results could not be reproduced. As experimentally found by Elemans (1989) a supercritical simple shear flow stabilizes the extending drops. Probably, Grace considered endpinching (drop by drop breakage from both ends of the thread) in stead of complete disintegration of the thread.

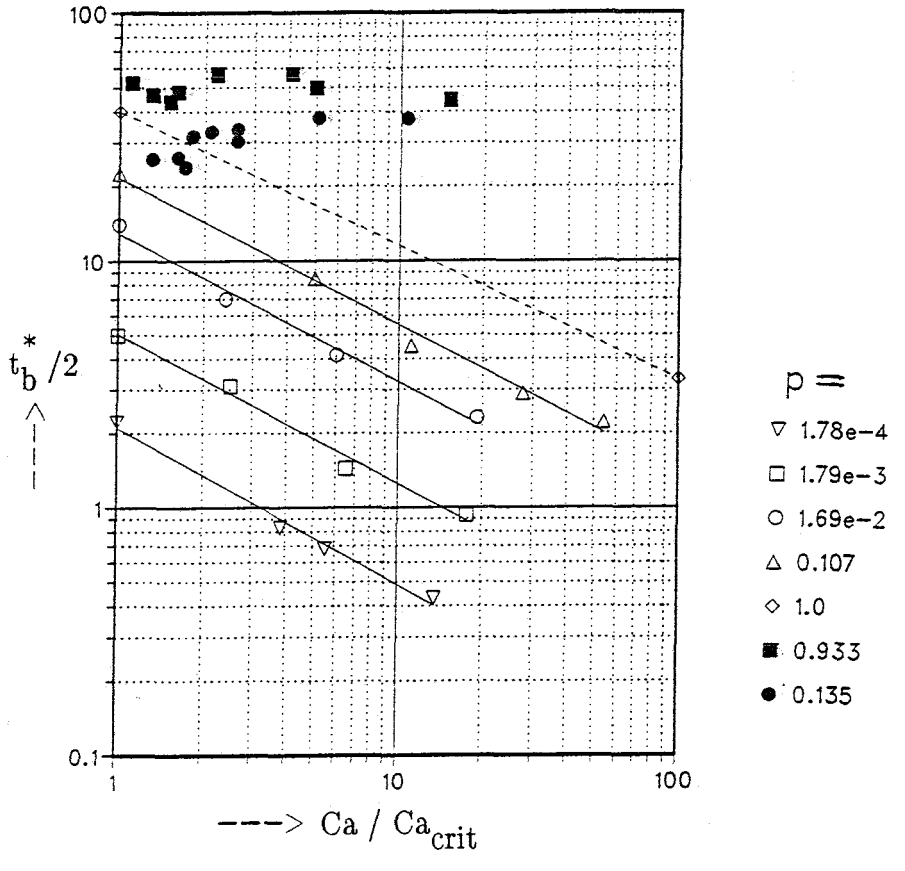

Figure 4.30 *Dimensionless time (Equation 4.30) for drop breakup in supercritical simple shear (open symbols Grace 1971; solid symbols Elemans 1989).*

In fact, the parameters along the axes of Figure 4.30 are quite arbitrary, since the figure combines three distinguishable stages of the experiment. The first stage is the initial deformation of the main drop, that takes more time as Ca reduces to Ca_{crit}*; the relevant timescale is* $t_\sigma = \eta_c R_{drop}/\sigma$*. The second stage contains the affine stretching of the unstable drop; the relevant timescale is* $t_G = 1/\dot{\gamma}$*. The last stage is the growth of the fatal disturbance (Figure 4.21), where* $t_\sigma = \eta_c R_{thread}/\sigma$ *is the relevant timescale. Consequently, it is not very conclusive to capture all three stages by only one dimensionless time, based on the first stage. Moreover, the breakup time is dependent on the initial dropsize, which, however, is fairly constant in most experiments with model liquids (~ 1 mm).*

Of great practical importance is the experimental evidence that affine deformation of the drop with the flow field indeed occurs if Ca_{crit} is sufficiently exceeded; see Figure 4.31 for plane hyperbolic flow as measured in the opposed jets device. The full curve corresponds to Equation 4.18, as in Figure 4.3. Apparently, at high enough values of the Capillary number ($Ca/Ca_{crit} > 10$) the shear stress dominates the interfacial stress completely when the drop is instantaneously subjected to the flow. Since these experiments involve a 2–D flow, affine deformation initially does not affect the width of the drop. A flattened ellipsoid results. As deformation proceeds, the cross section is contracted circular by the interfacial tension. According to Elemans (1989), in simple shear flow affine drop deformation already occurs at $Ca/Ca_{crit} > 2$, see Figure 4.32b.

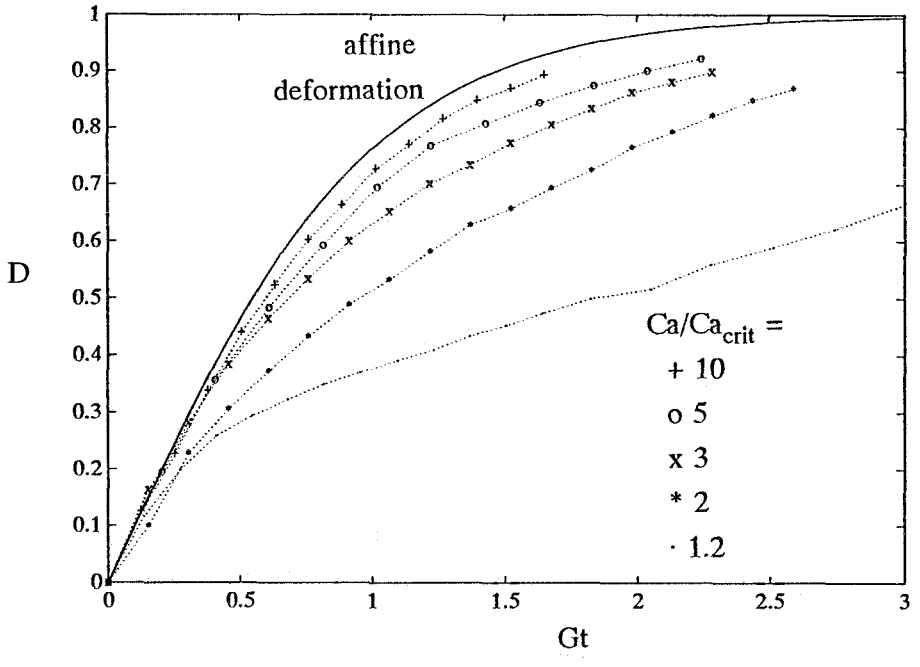

Figure 4.31 *Drop deformation D (= (L−B)/(L+B)) in supercritical plane hyperbolic flow as a function of the total applied deformation (or dimensionless time). The full curve corresponds to affine deformation, Equation 4.18. Castor oil drop and silicon oil matrix are both Newtonian, p = 0.19.*

At values of $Ca/Ca_{crit} < 1$, the drop deformation after a step in the shear rate approaches a constant value, see Figure 4.32a (This is the experimental procedure traditionally used to determine Ca_{crit}).

Similar results have been obtained for viscoelastic drops, although these need a somewhat larger excess of Ca_{crit} to be deformed affinely with the matrix. So, the elastic contribution makes the drops somewhat more difficult to deform than their viscous counterparts.

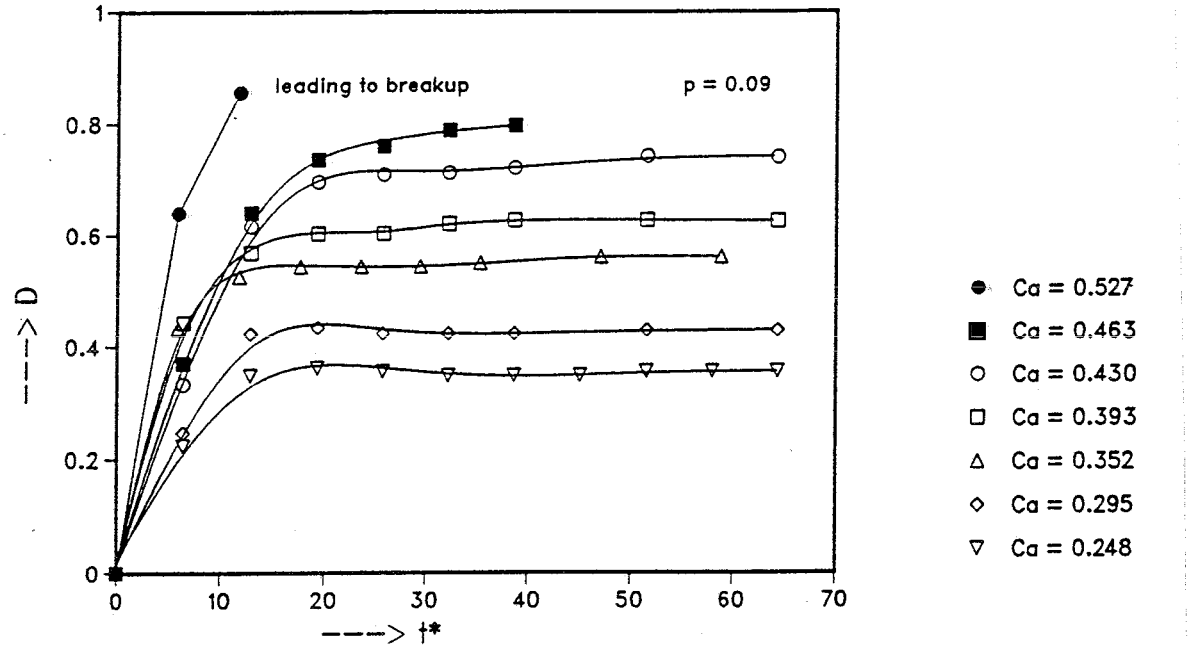

Figure 4.32 a *Progress of drop deformation in subcritical simple shear flow as a function of the dimensionless time (Equation 4.30). A stable equilibrium drop shape is obtained (Meijer and Bos 1989).*

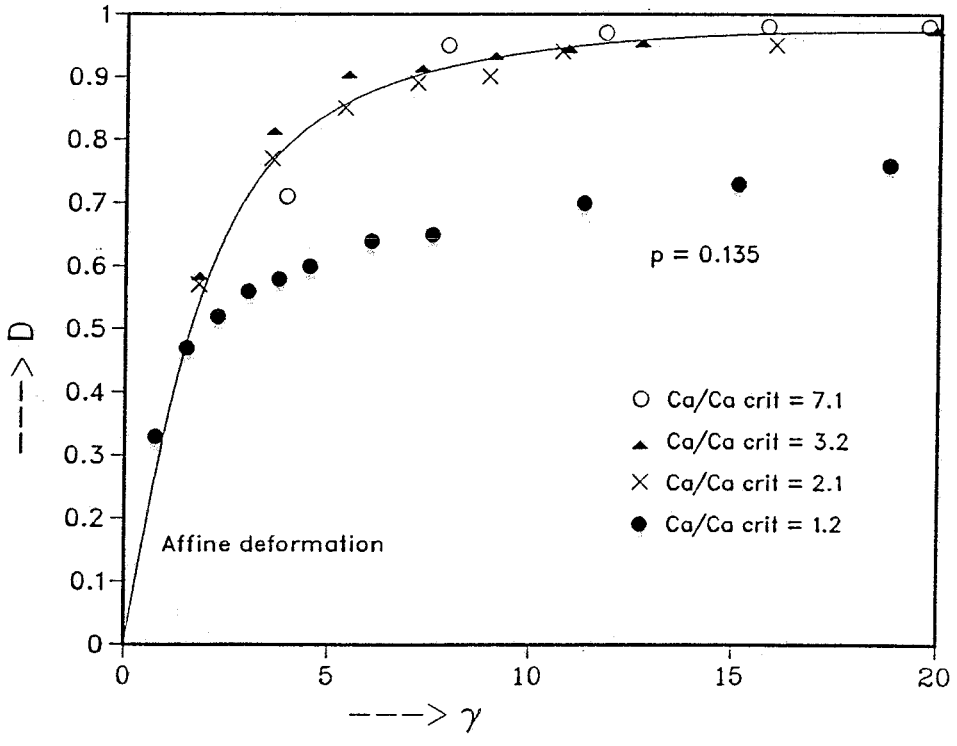

Figure 4.32 b *Drop deformation in supercritical simple shear flow as a function of the total applied deformation (or dimensionless time). The full curve corresponds to affine deformation, Equation 4.12 (Elemans 1989).*

The transient experiment shown in Figure 4.33 is realistic in the sense that it compares to the passage of a drop along a kneading flight of an extruderscrew, see Paragraph 4.6. A drop is stretched in an elongational flow and, after cessation of the flow, breaks via the so–called necking mechanism. Once the flow is stopped, two competitive processes proceed, both driven by the interfacial tension: (i) relaxation back to the original sphere and (ii) development of capillary waves, which is principally equivalent to the growth of Rayleigh disturbances on an infinite liquid thread. The overall relaxation of the drop is caused by the pressure difference over the interface (with principal radii of curvature R_1 and R_2):

$$\Delta p = \sigma \left[\frac{1}{R_1} + \frac{1}{R_2} \right] \qquad (4.46)$$

At the ends of the thread, where $R_1 = R_2 = R$, $\Delta p = 2\sigma/R$, while in the middle of the thread, where $R_1 = \infty$, $\Delta p = \sigma/R$. Thus, a pressure flow from the ends of the extended drop towards the centre is generated. Once a disturbance is present at the interface, also a pressure difference develops, according to the same Equation 4.46, between the centre of the disturbance (smallest diameter) and the bulbous ends (largest diameter). In the experiment of Figure 4.33 the timescale for the growth of disturbances apparently is smaller than that for overall relaxation. Note the satellite drop formed in the last stage of the process from the filament inbetween the two main drops.

As has been shown, in dispersive mixing both are important: shear rate and time. This in contrast with distributive mixing, where only the total shear and the number of reorientations or folds govern the process.

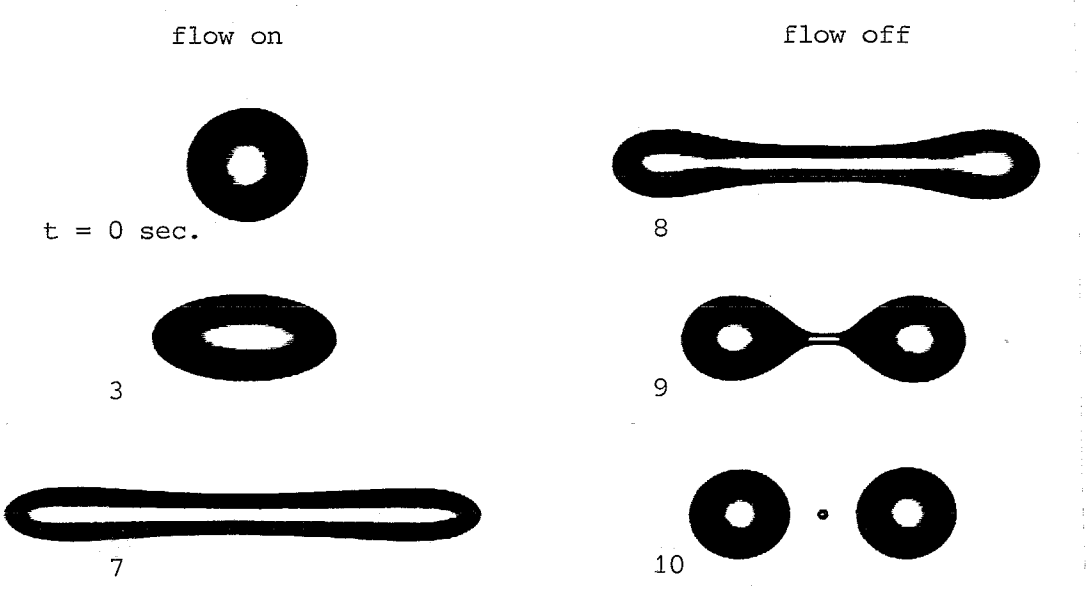

Figure 4.33 *Deformation of a 1.5 mm drop in the opposed jets device (2–D elongational flow) and breakup via necking after cessation of the flow. The castor oil drop and the silicon oil matrix both have a Newtonian viscosity of 0.7 Pa·s.*

In a number of figures the time has been made dimensionless with respect to the characteristic time for interfacial tension driven processes (Equation 4.30), $t_\sigma = \eta_c R/\sigma$. *If* t_σ *is compared with the characteristic time of the flow,* $t_G = 1/\dot{\gamma}$, *it follows that the Capillary number – defined before as the ratio between the shear stress and the interfacial stress – can also be interpreted as the ratio between these two characteristic times:*

$$Ca = \frac{t_\sigma}{t_G} = \frac{\eta_c \dot{\gamma} R}{\sigma} \qquad (4.47)$$

4.4.7 Numerical Simulations

Apart from experimental research, numerous numerical simulations of the dispersive mixing process have been performed, mostly for low Reynolds number flows. Some of the more recent studies will be summarized here. Khakhar and Ottino (1986) calculated Ca_{crit} as a function of the viscosity ratio p for all strong linear 2–D flows ($0 < \alpha \leq 1$, see Figure 4.25). In these quasi equilibrium calculations the criterion yields whether a stable drop shape exists in a specific shear field. In Figure 4.34 their numerical results are compared to the experiments of Grace (1971) and Bentley (1986 b). With his computer controlled four roll mill, Bentley (1985, 1986 a) could realize all combined flows with $0 < \alpha \leq 1$, by varying the speed of his rollers (diagonally) pair by pair.

It is remarkable that for moderate viscosity ratios both Bentley's and Khakhar's curves for the different types of flow practically reduce to one curve (Note that Bentley's results do not include simple shear flow, $\alpha = 0$). This cannot be recognized in the original figures of Bentley (1986 b) and Khakhar and Ottino (1986), since they define Ca as $\eta_c GR/\sigma$ rather than $\eta_c(1+\alpha)GR/\sigma$ (Equations 4.40–4.41). Their definition results in a bunch of curves.

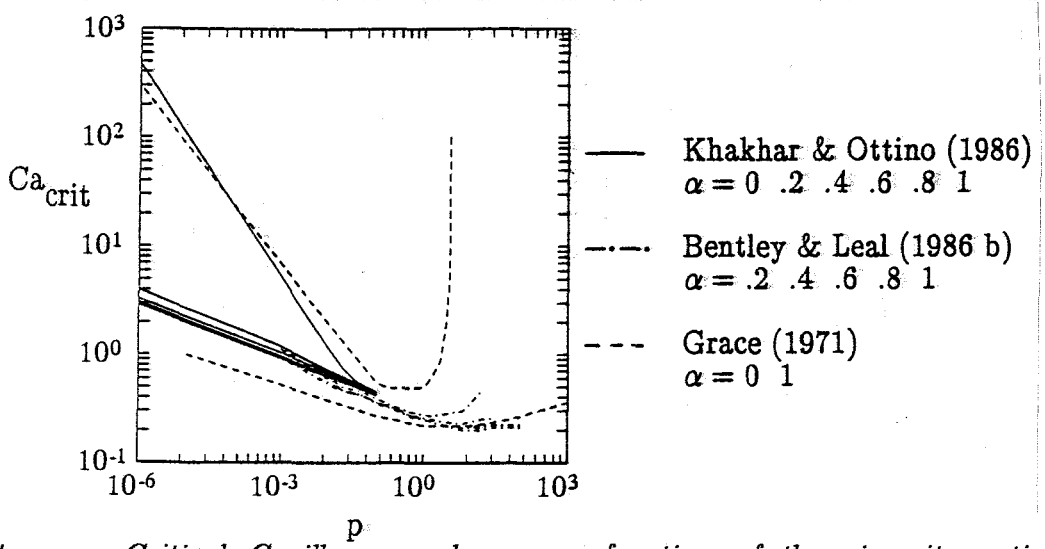

Figure 4.34 *Critical Capillary number as a function of the viscosity ratio for different types of flow (compare to Figure 4.26). Full lines are numerical results, dashed and dotted lines represent experimental results.*

Stone and Leal (1989 a,b) investigated several transient phenomena, using Newtonian liquids, both experimentally, using Bentley's apparatus, and numerically (for axisymmetric elongational flow), with an analysis based on the boundary integral method. Figure 4.35 shows the numerical results for an extended drop, relaxing towards equilibrium shape (sphere) in a quiescent matrix for different values of p. In their publications the simulations are compared to experiments such as in Figure 4.33. Once more, the competitive processes are overall relaxation towards a sphere and growth of capillary waves. Since the drops are extended quite far, growth of disturbances does not yield breakup by necking (breakage of a short thread via a dumbbell shape, see Figure 4.33) but by endpinching (drop by drop breaking from the ends of an intermediately long thread). Depending on the viscosity ratio p between drop and matrix and on the initial extension, either endpinching or overall relaxation dominates. The smaller the value of p, the faster the capillary waves develop resulting in endpinching.

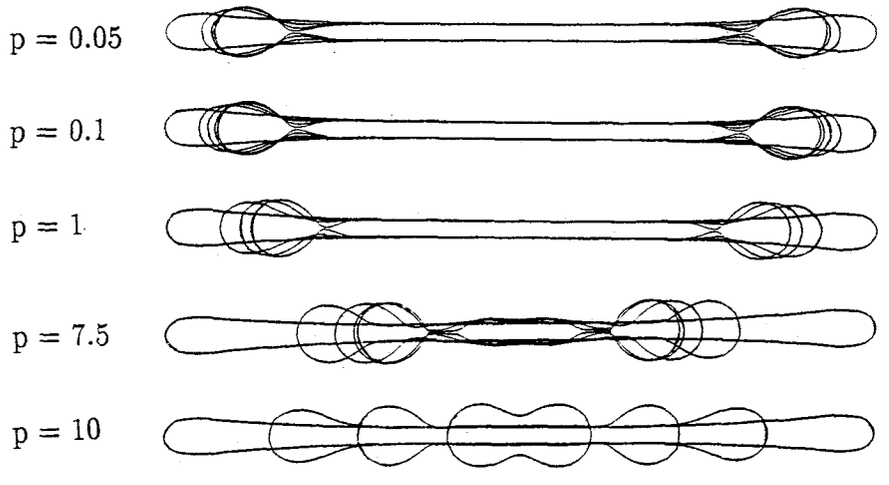

Figure 4.35 *Relaxation and breakup via endpinching of an initially extended drop in a quiescent matrix; the time steps between subsequent pictures increase with increasing viscosity ratio p (Stone and Leal 1989 a). Reprinted with permission of Cambridge University Press.*

A combination of simultaneously occuring processes is shown in Figure 4.36, where for p=1 initially only endpinching occurs, while at the end of the disintegration process, breakup via the more regular Rayleigh disturbances (the breaking mechanism for infinitely long threads) is found. In all these simulations, which compare extremely well to the experiments, the flow was stopped once the extension requested was reached (the initial shape of the extended drop was taken from the experiments).

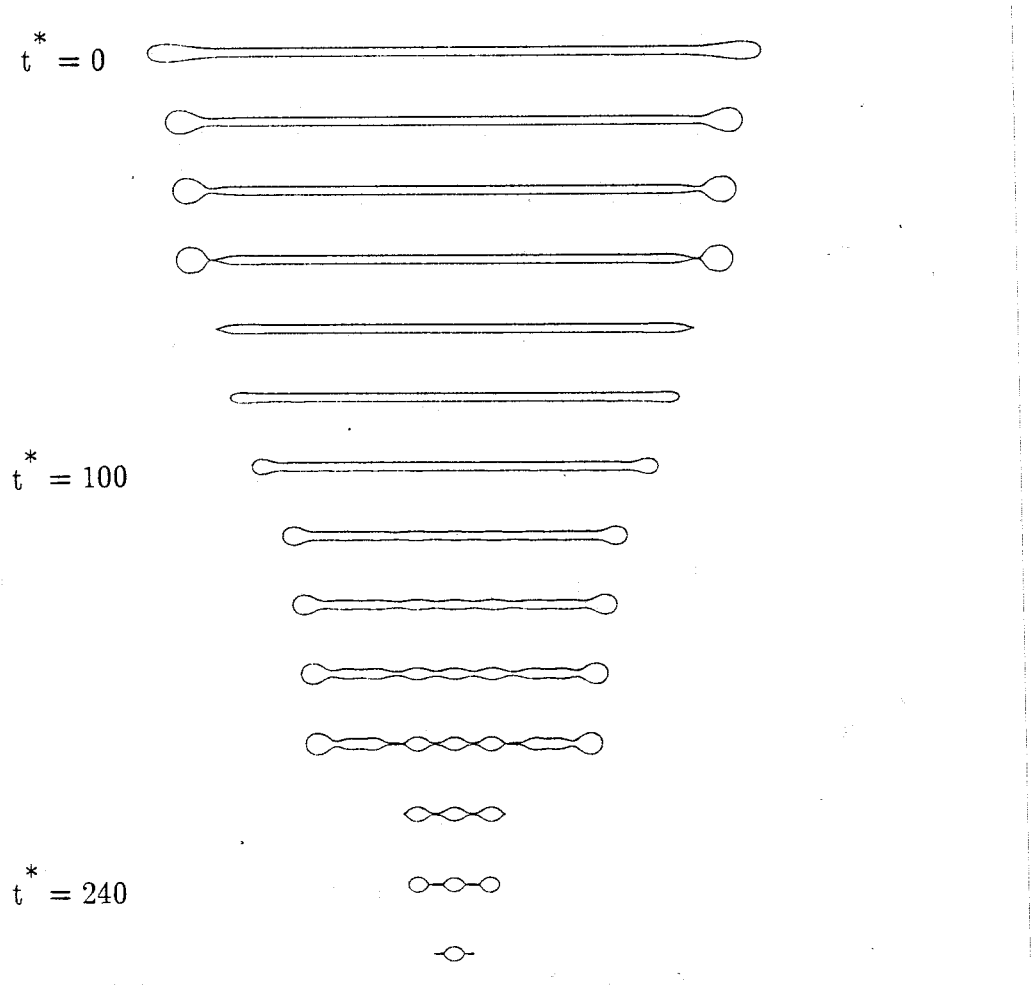

Figure 4.36 *Evolution of capillary waves (Rayleigh disturbances) during relaxation and breakup (via endpinching) of an initially highly extended drop in a quiescent matrix. Broken droplets are not shown in subsequent time steps (Stone and Leal 1989 a). Reprinted with permission of Cambridge University Press.*

Also a reduction of the shear rate to a non zero value below Ca_{crit} can be realized, see Figure 4.37. This figure shows the transient velocity field inside and around an initially extended drop during relaxation in an elongational flow field at 0.5 Ca_{crit}. At p = 1, necking occurs, while at p = 10 more time is needed to develop a disturbance and more extension will take place before breakup occurs.

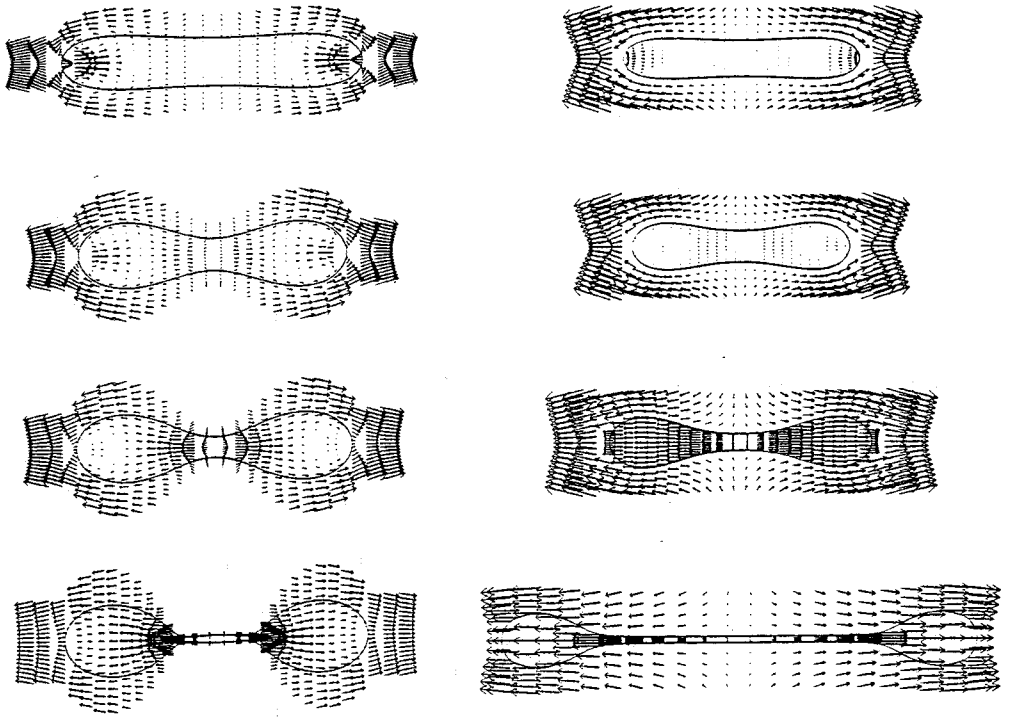

Figure 4.37 *Internal and external velocity fields during the relaxation and breakup of a drop after a step reduction in the Capillary number to 0.5 Ca_{crit}; the velocity vectors have been scaled differently for the two viscosity ratios (Stone and Leal 1989 b). Reprinted with permission of Cambridge University Press.*

Similar drop relaxation experiments with viscoelastic drops hardly show any difference as compared to Newtonian drops. The reason is the relatively (s)low deformation that does not yield serious molecular orientation (De << 1), in contrast to Figure 4.20b (De ≈ 1).

4.4.8 Continuum Modelling

At the end of this review on dispersive mixing, we address to the rigorous continuum modelling of Ottino's group. In this approach to mixing modelling (see Paragraph 4.3.5), also two phase flow with interfacial tension, affine deformation at $Ca/Ca_{crit} >> 1$ and disintegration of extended threads via the growth of Rayleigh disturbances can be incorporated. In their experiments, Tjahjadi and Ottino (1991) make use of an excentric Couette flow, the so–called journal bearing flow, which allows independent and discontinuous rotation of each rotor in either direction, see Figure 4.38.

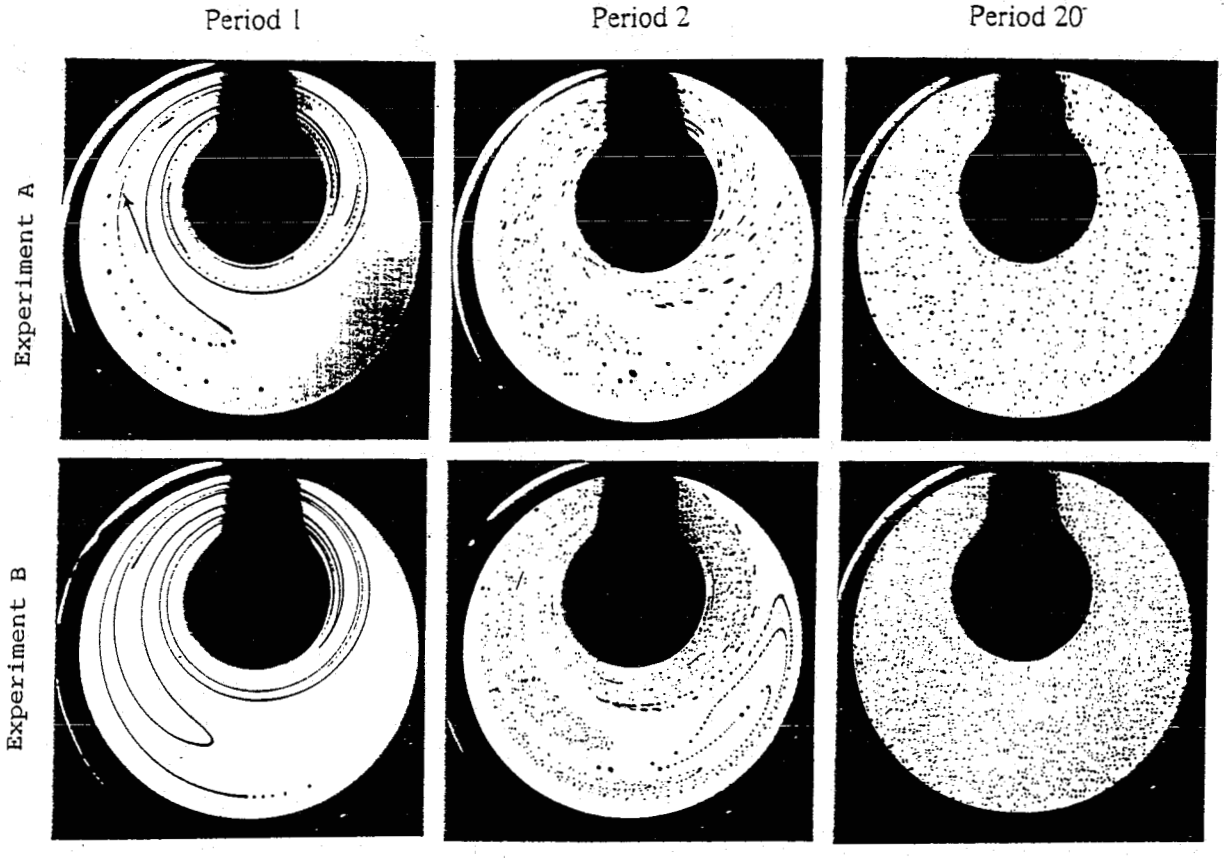

Figure 4.38 *Dispersive mixing in chaotic time periodic journal bearing flow; viscosity ratio is 0.01 in experiment A and 0.07 in B (Tjahjadi and Ottino 1991). Reprinted with permission of Cambridge University Press.*

A blob of a second (immiscible) liquid is extended, folded and deformed further via the flow induced by discontinuous rotor displacements. Via simulations, it is known a priori in which regions of the periodic flow high or low deformations and deformation rates can be realized. Depending on the timescale of the disintegration process, which strongly depends on the viscosity ratio, relatively thick threads break up already into big drops in the quiescent regions such as the folds. In the high shear regions the thread is continuously stretched counteracting the growth of Rayleigh disturbances (see Paragraph 4.4.3). It decreases in thickness until the growth rate of a disturbance with a smaller wavelength yields a local amplitude equal to the average radius of the thread that finally disintegrates. Because of the low value of p in experiment A, relatively thick threads quickly render big drops that breakup in subsequent stages of the mixing process. In experiment B, the viscosity ratio is higher and, consequently (smaller Ω_m, see Figure 4.19), the threads will decrease further in diameter before they disintegrate into smaller droplets, thus taking more time before breakup but yielding a finer dispersion via a one step disintegration process (see Figure 4.27). The comparison with theoretical predictions, see Tjahjadi and Ottino (1991), is amazingly correct. Clearly, all stages of the mixing process, from affine extension of large drops, via disintegration of threads, to deformation and breakup of relatively small drops, are present in this experiment which closely resembles a real mixing operation.

From this approach it might be concluded that, for Newtonian liquids, multiphase mixing in any 3–D transient flow can be numerically modelled, provided that sophisticated software and powerful hardware are available.

4.5. Coalescence

Until now, most of the fundamental research on the mixing of immiscible liquids concerned isolated drops. Most applications in polymer blending, and also in foodtechnology, only are of practical interest if at least 20% of the dispersed phase is present. Elmendorp (1986) concluded from experiments that already in the presence of a few percent of the dispersed phase coalescence becomes extremely important in immiscible polymer blends. At even higher volume fractions phase inversion occurs; the exact fraction strongly depends on the viscosity ratio p.

The phenomenon of phase inversion is easy to understand (stones in water will not easily change into water in stone, upon addition of stones), but difficult to model. Recently, a possible solution to the phase inversion problem has been suggested during the discussions on a conference after a lecture of Kraynik (1991), notably on computer modelling of the rheology of foam, see Reinelt and Kraynik (1990). In order to avoid too much extrapolation, however, only some important proven results on coalescence are reviewed here.

Important in the modelling of coalescence is knowledge of the volume fractions and the external flow field, since the chance on, or frequency of, the collision of drops, as well as the contact force and interaction time, are determined by these factors. For a number of simplified flows, expressions for these three parameters can be derived, see e.g. Chesters (1991). If two drops meet, they initially approach according to the global velocity field until their distance is of the order of their radius. From then, they influence the local flow field and the internal flow has to be taken into account. Prerequisite for coalescence is that the matrix material between the colliding drops is removed, see Figure 4.39.

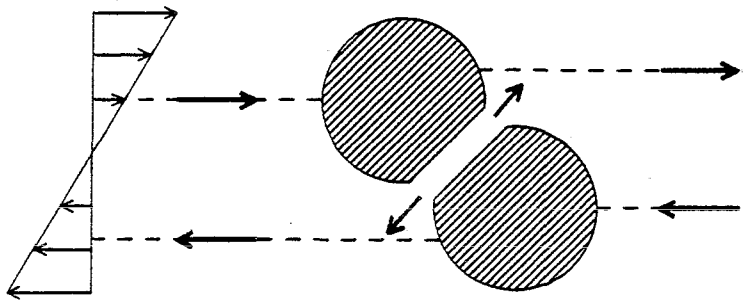

Figure 4.39 *Film drainage between two deformable colliding drops in simple shear.*

Once the liquid film is thin enough, instabilities rupture the film and the drops coalesce. If the critical filmthickness h_c, which is of the order of 50 Å, is not reached during the interaction time, the drops do not coalesce and separate. For coalescence of deformable drops in low Reynolds flows, the drainage of the liquid film is the rate determining step. Two extreme models are available for this viscous controlled film drainage: one starts with fully mobile interfaces, causing drag flow in the liquid film, the other with immobile interfaces, thus only pressure flow is generated. Figure 4.40 gives an impression of both extremes.

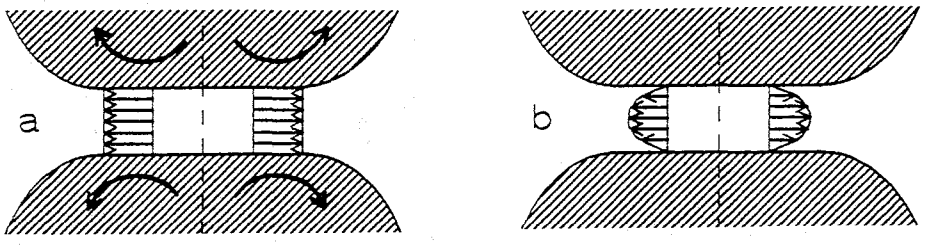

Figure 4.40 *Flow field in the liquid film between two deformable colliding drops for the case of a) fully mobile and b) immobile interfaces.*

For both models, the filmthickness h only asymptotically approaches zero and, after some time (the coalescence time t_c), reaches the critical thickness h_c, where filmrupture suddenly occurs. For fully mobile interfaces it is found:

$$t_c = \frac{3\eta_c R}{2\sigma} \ln\left[\frac{h_0}{h_c}\right] \qquad \Rightarrow t_c \sim R \ln R \qquad (4.48)$$

and for immobile interfaces:

$$t_c = \frac{3\eta_c R^2 F}{16\pi\sigma^2}\left[\frac{1}{h_c^2} - \frac{1}{h_0^2}\right] \qquad \Rightarrow t_c \sim F R^2 \qquad (4.49)$$

h_0 is the initial filmthickness at the start of the collision, which is basically unknown but can be approximated by the radius R; moreover $1/h_0^2$ is negligible, since $h_0 >> h_c$. Elmendorp (1986) showed, using immiscible polymer blends, that Equation 4.48 underpredicts the experimental coalescence time while Equation 4.49 gives an overprediction. The general trend that small drops coalesce much faster than big drops was however confirmed. Relatively recently, Chesters (1988, 1991) proposed a theory based on partially mobile interfaces. This model predicts coalescence times inbetween the two extremes:

$$t_c = \frac{\pi\eta_d F^{1/2}}{2(2\pi\sigma/R)^{3/2}}\left[\frac{1}{h_c} - \frac{1}{h_0}\right] \qquad \Rightarrow t_c \sim F^{1/2} R^{3/2} \qquad (4.50)$$

The validity of Chesters' model is restricted; for $p >> 1$, the model for immobile interfaces is the relevant one, while for $p << 1$ the model for fully mobile interfaces should be used (Moreover, if η_d is too low, the film drainage becomes inertia controlled). Chesters' model is the only one of the three available models that contains η_d rather than η_c. It is in reasonable consonance with Elemans' (1989) results and, at least qualitatively, predicts the experimentally determined influence of the absolute value of the viscosity of the dispersed phase η_d (van Gisbergen and Meijer 1991).

Apparently, both the mobility of the interface and the viscosity of the dispersed phase influence the flow inside the drops and thus the drainage rate of the liquid film inbetween. In polymer blends, compatibilizers, such as diblock copolymers, added to the system could immobilize the interface and, moreover, prevent too close an approach during collision of drops. The less coarse morphology, usually experienced when compatibilizers are added (thus σ decreased), is consequently due to (i) a delay of thread breakup because of a lower driving force yielding thinner threads and thus smaller droplets, (ii) an increase of the local Capillary number enabling the flow to break even smaller droplets before the limit Ca_{crit} is reached, and (iii) a prevention of coalescence.

In contrast to emulsions and low molecular weight suspensions, not enough attention has been paid to fully understand the influence of compatibilizers in polymer blends, despite the overwhelming amount of literature on polymer blending, reactive extrusion and the synthesis of diblock copolymers, tapered or regular, with different molecular weights. One of the reasons is that, e.g. concerning the molecular weight of the two blocks, contradictory demands exist for example with respect to the prevention of micel formation, migration rate towards the interface, and effective adhesion in the solid state. The results of van Gisbergen et al. (1990, 1991), showing a substantial increase of impact strength of Polystyrene / Ethylene–Propylene rubber blends, with a diblock copolymer added, after irradiation with an Electron Beam in the solid state (!), demonstrate that less obvious routes might be of particular interest in this field.

A contradiction seems to be present, concerning the influence of the contact force, since an increase in F results, according to the last two models for film drainage, in an increase of t_c. The reason is, however, that an increase in F causes an increase of the flattened area between the two deformable colliding drops, thus more liquid has to be removed over a larger distance. An important consequence of the relation between contact force and

coalescence time is that, during mixing, in regions of high deformation rates (thus high contact forces, but small interaction times) no coalescence will occur, although the collision frequency is high. Because of the high Capillary numbers in these regions, deformation of the drops, finally yielding breakup, will take place there. This in contrast with the more quiescent regions of the flow where no deformation but the more coalescence will occur. This feature can also be expressed in terms of the coalescence probability P_c, usually defined as:

$$P_c = \exp(-t_c/t_i) \tag{4.51}$$

where t_c is the time required for coalescence and t_i the interaction time $(1/\dot{\gamma})$. In simple shear flow Chesters' (1991) model for partially mobile interfaces predicts:

$$P_c = \exp\left[-c_1 \frac{R}{h_c} p\, Ca^{3/2}\right] \tag{4.52}$$

with c_1 an unknown constant of order unity. From this equation it is clear that coalescence is favoured by (i) small drop radii, (ii) low drop viscosity, and (iii) low Capillary number (i.e. low matrix viscosity, low shear rate, or high interfacial tension leading to a smaller flattened area).

The final morphology of a blend is the result of the dynamic equilibrium between breakup of the bigger drops (Ca large) and coalescence of the smaller ones (P_c large) during mixing. Both processes occur preferentially in different flow regions of the mixer. As a consequence, the influence of different processing conditions – like screw design, shear rate and residence time, but even the quenching conditions after the mixing process – on the morphogy of a blend might be substantial.

4.6. Polymer Blending in Practice

In this paragraph, an example is given of a single small dispersed drop passing a kneading flight in an extruder, in fact a transient flow situation, compare to Figure 4.33. Typically, the size and operating conditions of laboratory equipment are chosen, although scale up to industrial size is easy to realize. The screw, with a diameter $D = 25$ mm, can be one of the screws of a corotating twin screw extruder, part of the metering section of a single screw extruder, or basically part of any continuous or discontinuous mixing apparatus. Channel depth $H = 4$ mm, length $L/D = 5$, flight clearance $\delta = 0.2$ mm, and flight width $B = 4$ mm. At a screw speed $N = 400$ rpm, the shear rate over the flight is typically:

$$\dot{\gamma} = \frac{V}{\delta} = \frac{\pi DN}{60\,\delta} \approx 2500\ \mathrm{s}^{-1} \tag{4.53}$$

As a model system, PS, with a viscosity at this shear rate $\eta_d = 100$ Pa·s, is dispersed in HDPE, $\eta_c = 150$ Pa·s; therefore p ≈ 0.7, while the interfacial tension between PS and HDPE at the mixing temperature of 200°C equals $\sigma = 5 \cdot 10^{-3}$ N/m. The local Capillary number for a drop with diameter a = 2 μm equals:

$$\mathrm{Ca} = \frac{\eta_c \dot{\gamma} \mathrm{R}}{\sigma} = 75 \tag{4.54}$$

The residence time in the gap between flight and barrel wall is small, however:

$$\mathrm{t} = \frac{B}{V} \approx 8 \cdot 10^{-3}\ \mathrm{s} \tag{4.55}$$

which yields a dimensionless residence time:

$$t^* = t\frac{\sigma}{\eta_c R} = 0.3 \tag{4.56}$$

Although Ca_{crit} is largely surpassed (see Figure 4.26), the residence time is too short for completion of breakup, see Figure 4.30. Because $Ca >> Ca_{crit}$, affine deformation of the drop results. With the total shear in the clearance:

$$\gamma = \dot{\gamma}t = 20 \tag{4.57}$$

the length L and width B of the extended drop, after the passage, equal according to Equations 4.13–4.14:

$$L/a \approx \gamma = 20 \quad \Rightarrow L = 40\ \mu m \tag{4.58}$$

$$B/a \approx \gamma^{-1/2} = 0.2 \quad \Rightarrow B = 0.4\ \mu m \tag{4.59}$$

The shear rate in the screw channel is much lower:

$$\dot{\gamma} = \frac{\pi DN}{60H} = 125\ s^{-1} \tag{4.60}$$

At a typical throughput $Q = 5.10^{-6}\ m^3/s$, the residence time in the screw channel equals:

$$t = \frac{\pi DLH}{Q} = 8\ s \tag{4.61}$$

This time is sufficient for the disintegration of the thread (extended drop) via Rayleigh disturbances, see Equation 4.29. The final number and size of the droplets formed can be estimated from Equation 4.32 and roughly yields 15 droplets of 0.8 μm.

This simple example clearly illustrates that usual gapsizes are more than sufficient for breakup of even the smallest drops, albeit via a different sequence of local processes than generally thought. Standard compounding does not yield fine dispersions as predicted by this simple application of the existing knowledge of dispersive mixing. An obvious reason is the presence of coalescence, the importance of which was already stressed in the previous paragraph. Another cause is that not all material might pass the high shear region, as already clearly illustrated in the simplified modelling of the dispersive mixing of carbon black in rubber, using Banbury type of batch mixers, see Manas et al. (1982, 1984). Since not only in batch mixers, but also in continuous extruders, the frequency of passages through the high shear section in the circulating flow directly depends on the gapsize, it sometimes might be wise to use worn screws. Manas et al. came to the same result, provided that the viscosity of the matrix was large enough to yield a shear stress which is bigger than the cohesive stress, even for non−optimal oriented particles. In the case of mixing immiscible liquids, a detailed investigation of the influence of Ca, p and t^*, but especially of the viscoelasticity of the dispersed phase on deformation and breakup during the passage through a narrow gap (i.e. transient flow conditions), could give more precise conditions for the optimal gapsize.

In the practice of polymer blending, experimental evidence of the sequence of local processes in mixing of immiscible liquids can be found. A beautiful example is given in Figure 4.41, which shows a longitudinal section of a part of the strand formed after leaving the die of a corotating twin screw extruder. The blend consists of the model system PS/HDPE. Figure 4.41a was obtained, of course after staining, from a directly quenched strand. The matrix is HDPE; the extended filaments of PS have been formed in the converging flow to the die; hardly time for either disintegration of the filaments or coalescence was available. Figure 4.41b shows the same strand, now quenched only after a few seconds residence in the circumventing air by increasing the distance between the die and the waterbath somewhat. Disintegration of the thinner threads into lines of droplets

now has been completed. Notice the order of magnitude of the final dropletsize, compared to the prediction from the calculations in the simple example treated above.

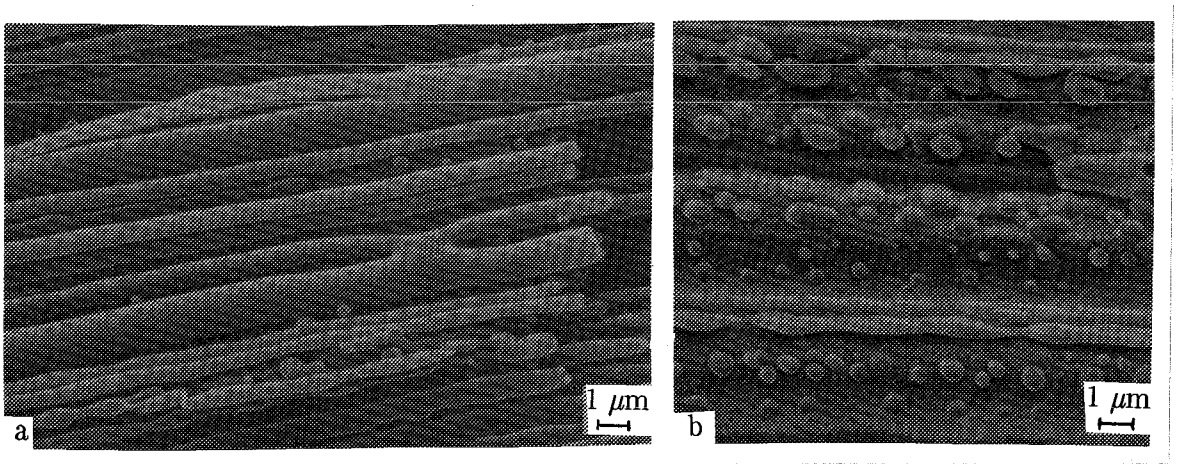

Figure 4.41 *Breaking PS threads in a HDPE matrix. The blends were prepared using a corotating twin screw extruder with: a) quenching immediately after the die or b) several seconds between die and waterbath (Meijer et al. 1988). Reprinted with permission of Hüthig und Wepf Verlag.*

4.7. Conclusions

In the initial stages of mixing of immiscible liquids, the typical lengthscale of the minor component is such large that $Ca >> Ca_{crit}$ and mixing is only distributive (passive interfaces). The deformation of disperded drops is affine, just as if the liquids were miscible, only the total shear matters. Most important is the introduction of periodic folds via a practical realization of the baker's transformation, yielding an exponential increase of the interfacial area with total shear rather than a linear increase. In the analyses and design of efficient mixing equipment, attention should particularly be focussed on the avoidance of regular islands: regions in the flow that do not effectively deform, but only translate and rotate, since mixing quality is always determined by the non–mixed fraction.

The affine deformation in the flow causes the drops to extend into long slender threads, until local radii are reduced such that $Ca \approx Ca_{crit}$ (≈ 1). The liquid threads become unstable and disintegrate caused by interfacial tension driven processes (active interfaces). The most important mechanisms are the growth of uniform Rayleigh disturbances in the mid part of the thread, endpinching at both ends, retraction, and necking in case of relatively short dumbbell shaped threads. During dispersive mixing deformation rate and time are not interchangeable such as in distributive mixing where only the total shear is of importance. Therefore attention should be paid to the timescales of the competitive processes which strongly depend on the viscosity ratio and on the elastic properties of especially the dispersed phase. Quasi equilibrium data can give evidence whether drops once formed will deform further leading to breakup or whether they will reach a stable deformed shape. Interestingly, the final results in terms of the average dropletsize of a fast deformation in a high shear region, sustained long enough to yield extremely large drop deformations, followed by disintegration of the ultrafine threads formed, in a quiescent region of the flow, should not necessarily be the same as a step by step process of repeated

extension and breakup, for the same total energy consumed in the mixing process.

A morphology once formed may coarsen due to coalescence of colliding drops of the dispersed phase. Apart from the volume fractions of the constituents and the flow field externally applied by the mixer, the viscosities of both phases, the interfacial tension, and the mobility of the interfaces are the parameters that govern the mechanism of coalescence. In viscous controlled coalescence, the rate determining step is the drainage of the liquid film between the, somewhat flattened, colliding drops. From simple theories it can be seen that, in contrast to drop breakup, coalescence occurs in quiescent regions rather than in high shear (rate) zones. If a collision proceeds too fast, the liquid film has not yet drained sufficiently to disrupt and the drops separate.

Application of the existing theories to blending of polymer melts, requires an extension of the research to viscoelastic liquids. Although a number of discrepancies can be found in the results of different researchers (Flumerfelt 1972, Chin and Han 1979 and 1980, Goren and Gottlieb 1982, Bousfield et al. 1986, Cruz–Mena et al. 1988 and de Bruijn 1989), experiments in our laboratory indicate that viscoelasticity has a pronounced effect on especially the timescale of the different processes involved in mixing if both the deformation and the deformation rate are sufficiently large (De large).

Most results of the theoretical and experimental research on the different stages of the mixing process are expressed in dimensionless numbers, like Ca, p, γ, t^*, D etc. In principle, an extrapolation of the results obtained with model liquids to practical systems with polymer melts is possible. Moreover, it has been shown that relatively simple experiments and restrictive models of elementary steps may already yield conclusive results. Apart from further refinement, a connection of the various models into an overall theory is an interesting challenge for future research.

4.8. References

Acrivos A.; 4th Int. Conf. on Physiochemical Hydrodynamics, Ann. N.Y. Acad. Sci., Vol. 404, p.1 (1983).

Bentley B.J.; Ph.D. Thesis, California Inst. of Technology, Pasadena California (1985).

Bentley B.J., Leal L.G.; J. Fluid Mech., Vol. 167, p. 219 (1986 a).

Bentley B.J., Leal L.G.; J. Fluid Mech., Vol. 167, p. 241 (1986 b).

Bousfield D.W., Keunings R., Marrucci G., Denn M.M.; JNNFM, Vol. 21, p. 79 (1986).

Bruijn R.A. de; Ph.D. Thesis, TU Eindhoven (1989).

Bruijn R.A. de; Preprints of IACIS conf./ EFCE event 439 'The Preparation of Dispersions' p. 103, Veldhoven The Netherlands, October 14–16 (1991); to appear in Chem. Eng. Sci., Vol. 48 (1992/1993).

Carriere C.J., Cohen A.; J. Rheol., Vol. 35 (2), p. 205 (1991).

Catchpole J., Fulfort G.D.; in: Fluid Mechanics Source Book, Dimensionless Groups, Ed. Parker S.P., McGraw Hill, London, p. 158 (1988).

Chappelear D.C.; Polym. Preprints 5, p. 363 (1964).

Chella R., Ottino, J.M.; Ind. Eng. Chem. Fund., Vol. 24, p. 170 (1985).

Chesters A.K.; Euromech 234, Int. Conf. Turbulent Two Phase Flow Systems, Toulouse France (1988).

Chesters A.K.; Trans IChemE, Vol. 69 Part A, p. 259, (1991).

Chin H.B., Han C.D.; J. Rheol., Vol. 23 (5), p. 557 (1979).

Chin H.B., Han C.D.; J. Rheol., Vol. 24 (1), p. 1 (1980).

Cruz–Mena J., Serrania F., Mena B.; Progress and Trends in Rheology II, p. 262 (1988).

Einstein A.; Ann. Physik, Vol. 19, p. 289 (1906) and Vol. 34, p. 591 (1911).

Elemans P.H.M.; Ph.D. Thesis, TU Eindhoven (1989).

Elemans P.H.M., Janssen J.M.H., Meijer H.E.H.; J. Rheol., Vol. 34 (8), p. 1311 (1990).

Elemans P.H.M.; Chapter 10 in Encyclopedia of Fluid Mech., Ed. Cheremisinoff N.P., Vol. 9 Pol. Flow Eng. (1990).

Elemans P.H.M., Bos H.L., Janssen J.M.H., Meijer H.E.H.; Preprints of IACIS conf./ EFCE event 439 'The Preparation of Dispersions' p. 111, Veldhoven The Nether–lands, October 14–16 (1991); to appear in Chem. Eng. Sci., Vol. 48 (1992/1993).

Elmendorp J.J.; Ph.D. Thesis, TU Delft (1986).

Flumerfelt R.W.; Ind. Eng. Chem. Fundam., Vol. 11 (3), p. 312 (1972).

Fuller G.G., Leal L.G.; J. Polym Sci, Polym. Phys. Ed., Vol. 19, p. 557 (1981).

Ghosh A.K., Ranganathan S., Lindt J.T., Lorek S.; Antec '91 Montreal, Soc. Plast. Eng., p. 232 (1991).

Giesekus H.; Rheol. Acta, Band 2, Heft 2, p. 112 (1962).

Gisbergen J. van, Borgmans C.P.J.H., Sanden M.C.M. van der, Lemstra P.J.; Polymer Commun., Vol. 31, p. 161 (1990).

Gisbergen J. van; Ph.D. Thesis, TU Eindhoven (1991).

Gisbergen J. van, Meijer H.E.H.; J. Rheol., Vol. 35 (1), p. 63 (1991).

Gisbergen J. van, Sanden M.C.M. van der, Haan J.W. de, Ven L.J.M. van de, Lemstra P.J. Makromol. Chem. Makromol. Symp., Vol. 41, p. 153 (1991).

Gordon J.E.; The New Science of Strong Materials, or Why You Don't Fall Through the Floor, Chapter 10, Penguin, London, (1968, 1978).

Gordon J.E.; Structures, or Why Things Don't Fall Down, Penguin, London (1978).

Goren S.L., Gottlieb M.; J. Fluid Mech., Vol. 120, p. 245 (1982).

Grace H.P.; Eng. Found. Res. Conference Mixing, 3rd Andover, N.H. (1971), republished in Chem. Eng. Commun., Vol. 14, p. 225 (1982).

Janssen J.M.H.; AIO–2 Report, TU Eindhoven, WFW 91.8, (1991).

Janssen J.M.H., Peters G.W.M., Meijer H.E.H.; Preprints of IACIS conf./ EFCE event 439 'The Preparation of Dispersions' p. 121, Veldhoven The Netherlands, October 14–16 (1991); to appear in Chem. Eng. Sci., Vol. 48 (1992/1993).

Khakhar D.V., Ottino J.M.; J. Fluid Mech., Vol. 166, p. 265 (1986).

Khakhar D.V., Ottino J.M.; Int. J. Multiphase Flow, Vol. 13 no 1, p. 71 (1987).

Kraynik A.M.; Lecture on PPS 7 Conference, Hamilton, Canada (April 1991).

Kuhn W.; Kolloïd Z., Vol. 132, p. 84 (1953).

Leong C.W., Ottino J.M.; J. Fluid Mech., Vol. 209, p. 463 (1989).

Manas–Zloczower I., Nir A., Tadmor Z.; Rubber Chem. Techn., Vol. 55, p. 1250 (1982).

Manas–Zloczower I., Nir A., Tadmor Z.; Rubber Chem. Techn., Vol. 57, p. 583 (1984).

Meijer H.E.H., Bos H.L.; in: Extruder im Extrusionsprozess (in German), p. 59, VDI–Verl. Düsseldorf (1989), also Academic Seminar: Current Situation and Topics of Pol. Proc. Techn. (in English), p. 39, JP90 Tokyo (1990), and Seikei–Kakou (in Japanese), J. of JPPS, Vol. 3 (1), p. 33 (1991).

Meijer H.E.H., Lemstra P.J., Elemans P.H.M.; Makromol. Chem., Macromol. Symp., Vol. 16, p. 113 (1988).

Mikami T., Cox R., Mason R.G.; Int. J. Multiphase Flow, Vol. 2, p. 113 (1975).

Milliken W.J., Leal L.G.; JNNFM, Vol. 40, p. 355 (1991).

Milliken W.J., Leal L.G.; JNNFM, Vol. 42, p. 231 (1992).

Ng K.Y., Erwin L.; Polym. Eng. Sci., Vol. 21, p. 4 (1981).

Olbricht W.L., Rallison J.M., Leal L.G.; JNNFM, Vol. 10, p. 291 (1982).

Ottino J.M., Chella R.; Pol. Eng. Sci., Vol. 23, p. 7 (1983).

Ottino J.M.; The Kinematics of Mixing: Stretching, Chaos and Transport, Cambridge Univ. Press, Cambridge (1989).

Ottino J.M.; Ann. Rev. Fluid Mech., Vol. 22, p. 207 (1990).

Ottino J.M.; Phys. Fluids, Vol. A3 (5), p. 1417 (1991).

Palierne J.F., Lequeux F.; JNNFM, Vol. 40, p. 289 (1991).

Prigogine I., Stengers I.; Order out of Chaos, Flamingo, Glasgow (1984).

Rallison J.M.; Ann. Rev. Fluid Mech., Vol. 16, p. 45 (1984).

Rayleigh Lord; Proc. R. Soc., (London) Vol. 29, p. 71 (1879).

Reinelt D.A., Kraynik A.M.; J. Fluid Mech., Vol. 215, p. 431 (1990).

Rumscheidt F.D., Mason S.G.; J. Coll. Sci., Vol. 16, p. 238 (1961).

Schilo D., Ostertag, K.; Verfahrenstechnik (in German), Vol. 6, 2, p.45 (1972).

Sluijters R.; De Ingenieur (in Dutch), Vol. 77, 15, p. 33 (1965).

Stone H.A., Bentley B.J., Leal L.G.; J. Fluid Mech., Vol. 173, p. 131 (1986).

Stone H.A., Leal L.G.; J. Fluid Mech., Vol. 198, p. 399 (1989 a).

Stone H.A., Leal L.G.; J. Fluid Mech., Vol. 206, p. 223 (1989 b).

Tanner R.I.; AIChE J., Vol. 22, 5, p. 910 (1976).

Taylor G.I.; Proc. R. Soc., (London) Vol. A 138, p. 41 (1932).

Taylor G.I.; Proc. R. Soc., (London) Vol. A 146, p. 501 (1934).

Tjahjadi M., Ottino J.M.; J. Fluid Mech., Vol. 232, p. 191 (1991).

Tjahjadi M., Stone H.A., Ottino J.M.; to appear in J. Fluid Mech. (1992).

Tomotika S.; Proc. R. Soc., (London) Vol. A 150, p. 322 (1935).

Tomotika S.; Proc. R. Soc., (London) Vol. A 153, p. 302 (1936).

Weber C.; Z. Angew. Math. Mech., Vol. 11, p. 136 (1931).

Appendix 4.A. Determination of Interfacial Tension

Many methods have been developed to measure the interfacial tension between two immiscible liquids. For polymer systems, the spinning drop and, in different experimental setups, the pendent drop are frequently used. Carriere and Cohen (1991) use a technique for the determination of interfacial tensions, based on the relaxation of a deformed drop back to a sphere. They embed a short fibre in a matrix, heat the system and analyse the progress of the relaxation to a sphere. Since thick and short fibres are used, the timescale for the evolution of capillary Rayleigh instabilities is not reached within their experiments, that may last for even a few hours.

In this review, the growth rate of Rayleigh disturbances, caused by the interfacial tension, has been summarized and it has been noticed that the quantitative theory of Tomotika for Newtonian liquids was already developed in 1935. Knowing that polymer melts are by far ideal Newtonian liquids, but realising that as long as the deformation rate is small, thus the typical process time t is long, compared to the relaxation time θ of the melts (Deborah number $De = \theta/t << 1$), the zero shear viscosities can be used and the problem can be inverted: From the growth rate of the disturbances on an infinite thread, the interfacial tension can be determined, see Elemans et al. (1990). Provided that no yield stress is present and somewhat care is taken in the sample preparation (uniformity of the thread, length to diameter long enough to prevent a disturbing influence of endpinching), this easy, flexible method gives reproducible results, without requiring accurate information on the densities of the polymers at the experimental, high temperatures.

A thread of one polymer with a diameter of, for example, 20 μm obtained from a meltindexer, a Fanno process (tubeless spinning) from a molten granule, or from a somewhat more sophisticated spinning process, is placed between two films of the other

polymer at roomtemperature. The system is subsequently heated in a hot stage probe of a microscope. Since everything is slow (an experiment may reach from several minutes to a few hours, depending on the diameter of the thread, the viscosities and the interfacial tension), residual stresses, if present, will easily relax during the heating step. Monitoring of the growth of the disturbances as a function of time (videotaping is instructive but simple photos are sufficient) and plotting the amplitudes on a semilogarithmic scale, directly yields the growth rate q from the slope of the line, compare Equation 4.24. See Figure 4.A.1.

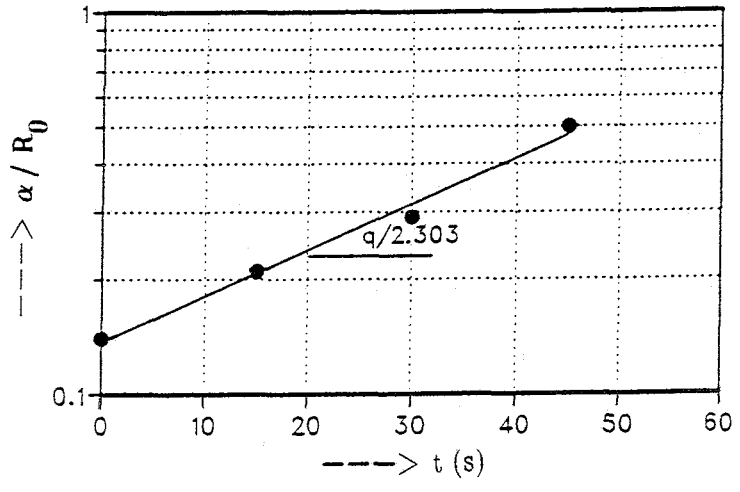

Figure 4.A.1 *Plot of the relative amplitude versus time for the PA-6 thread ($2R_0$ = 55 μm, η_d = 425 Pa·s) in Figure 4.16, in a PS matrix (η_c = 1000 Pa·s) at 230°C. Experimental and theoretical dominant wavenumber are close: 0.60 and 0.61 (Elemans et al. 1990).*

From this growth rate, using Equation 4.25, the interfacial tension can be obtained:

$$\sigma = \frac{2\,q\,\eta_c R_0}{\Omega_m(\lambda_m, p)} \qquad (4.A.1)$$

No information on the initial disturbances is necessary, neither on the final disintegration time, which always will show a somewhat local character. Moreover, a direct test on the quality of the experiment is available, since the experimental wavenumber X ($= 2\pi R_0/\lambda$) must be identical to the theoretical dominant number X_m, see Figure 4.19.

The influence on the interfacial tension of the presence of a compatibilizer, can be experimentally determined via mixing the compatibilizer in the first polymer, prior to spinning. The results of an addition of a Styrene–(hydrogenated)Polybutadiene diblock copolymer to the model system HDPE/PS on the resulting interfacial tension, measured with this so–called breaking thread method, is given in Figure 4.A.2.

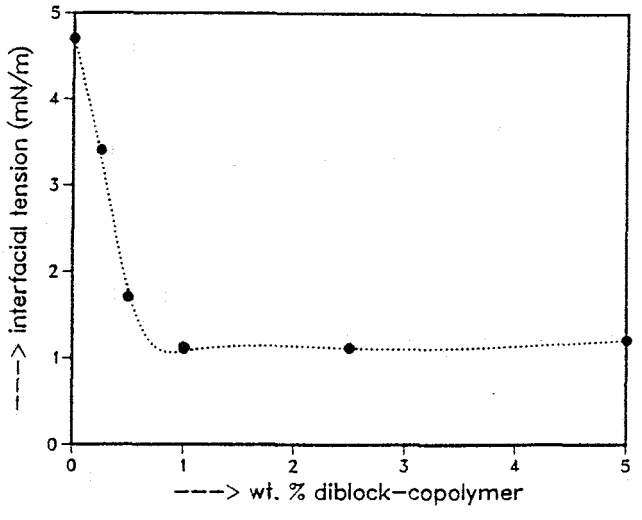

Figure 4.A.2 *Interfacial tension between PS matrix and HDPE thread (measured at 200°C using the breaking thread method) versus weight % of a diblock copolymer added to the thread phase (Elemans et al. 1990).*

No further decrease in interfacial tension is found if more than 1% compatibilizer is added. As expected, this is reflected in the final morphology of the blend after compounding as well, see Elemans (1989).

List of Symbols

A	interfacial area	[m^2]
A_0	initial interfacial area	[m^2]
a	diameter of a drop	[m]
B	width of a deformed drop	[m]
Ca	Capillary number ($\eta_c \dot{\gamma} R/\sigma$)	[–]
Ca_{crit}	critical Capillary number	[–]
D	drop deformation ((L–B)/(L+B))	[–]
De	Deborah number (θ/t)	[–]
e_f	efficiency of mixing	[–]
F	contact force	[N]
G	(scalar) velocity gradient	[1/s]
h	film thickness	[m]
h_c	critical film thickness	[m]
h_0	initial film thickness	[m]
k	Boltzmann's constant	[J/K]
L	length of a deformed drop	[m]
L	characteristic lengthscale	[m]
l_0	initial length	[m]
n	number of reorientations	[–]
n	number of mixing elements	[–]
p	viscosity ratio (η_d/η_c)	[–]
P_c	coalescence probability	[–]
Δp	pressure difference	[Pa]
q	growth rate of a disturbance	[1/s]
R	radius of a drop or thread	[m]

R_0	initial radius of a thread	[m]
$\overline{R}$	average radius of a disturbed thread	[m]
$R_{1,2}$	principal radii of curvature	[m]
Re	Reynolds number ($\rho UL/\eta$)	[–]
T	absolute temperature	[K]
t	time	[s]
t^*	dimensionless time (t/t_σ)	[–]
t_b	time untill breakup	[s]
t_b^*	dimensionless breakup time	[–]
t_c	coalescence time	[s]
t_G	characteristic time of the flow	[s]
t_i	interaction time	[s]
t_σ	char. time for σ–driven processes ($\eta_c R/\sigma$)	[s]
U	characteristic velocity	[m/s]
We_1	Weber number 1 ($\rho U^2 L/\sigma$)	[–]
X	wavenumber of a disturbance ($2\pi R_0/\lambda$)	[–]
X_m	dominant wavenumber	[–]
z	z–coordinate	[m]

B	flight width	[m]
D	screw diameter	[m]
δ	flight clearance	[m]
H	channel depth	[m]
L	extruder length	[m]
N	screw speed	[rpm]

Q	throughput	[m^3/s]
V	screw velocity	[m/s]
α	flow type parameter	[–]
α	amplitude of a disturbance	[m]
α_0	initial amplitude of a disturbance	[m]
α_b	amplitude at breakup	[m]
γ	shear	[–]
γ_{tot}	total shear	[–]
$\dot{\gamma}$	shear rate ($\sqrt{(2D:D)}$)	[1/s]
ϵ	strain	[–]
$\dot{\epsilon}$	elongation rate	[1/s]
η	viscosity	[Pa·s]
η_d	viscosity of the dispersed phase	[Pa·s]
η_c	viscosity of the continuous phase	[Pa·s]
η_0	viscosity of the solvent	[Pa·s]
θ	relaxation time of a liquid	[s]
λ	wavelength of a disturbance	[m]
λ_m	dominant wavelength	[m]
ρ	density	[kg/m^3]
σ	interfacial tension	[N/m]
τ	shear stress	[Pa]
ϕ	volume fraction spheres	[–]
Ω	dimensionless growth rate of a disturbance	[–]
Ω_m	dim.less growth rate of dominant disturbance	[–]

$\vec{u}$	velocity vector with components (u,v,w)	[m/s]
$\vec{x}$	position vector with components (x,y,z)	[m]
$\vec{\nabla}$	gradient operator	[1/m]
$\mathbf{C}$	right Cauchy–Green tensor ($\mathbf{F}^C \cdot \mathbf{F}$)	[–]
$\mathbf{D}$	rate of deformation tensor ($(\mathbf{L}+\mathbf{L}^C)/2$)	[1/s]
$\mathbf{F}$	deformation tensor	[–]
$\mathbf{L}$	velocity gradient tensor	[1/s]
$\mathbf{\Omega}$	spin tensor ($(\mathbf{L}-\mathbf{L}^C)/2$)	[1/s]